

Higher-point Energy Correlators: Factorization in the Back-to-Back Limit & Non-perturbative Effects

Ankita Budhraj,^a Isabelle Pels,^{a,b} Wouter J. Waalewijn^{a,b}

^a*Nikhef, Theory Group, Science Park 105, 1098 XG, Amsterdam, The Netherlands*

^b*Institute for Theoretical Physics Amsterdam and Delta Institute for Theoretical Physics, University of Amsterdam, Science Park 904, 1098 XH Amsterdam, The Netherlands*

E-mail: abudhraj@nikhef.nl, isabellepels01@gmail.com,
w.j.waalewijn@uva.nl

ABSTRACT: N -point energy correlators are powerful observables for studying strong interactions, with applications ranging from extractions of the strong coupling α_s to probes of jet modification in heavy-ion collisions and determination of the top-quark mass. Their practical use has, however, been limited by the complicated phase space for large N . Using a recently introduced parametrization that simplifies this structure, we study projected N -point correlators in two regimes: factorization in the back-to-back limit and leading non-perturbative effects in the collinear limit. While results in the back-to-back regime were previously limited to the energy-energy correlator, our approach allows us to derive the factorization theorem for arbitrary N . We compute the new ingredient, a one-loop jet function, needed for the next-to-next-to-leading-logarithmic resummation, which enables future α_s extractions with complementary systematics. We further determine the analytic structure of leading non-perturbative power corrections for arbitrary N , including their dependence on the center-of-mass energy Q , the value of N , and the angular scale x . We present the first results for non-integer $N < 1$, finding that the classical scaling in x acquires an N -dependent modification, and that a new non-perturbative matrix element $\tilde{\Omega}^{[N]}$ appears. In a certain approximation, $\tilde{\Omega}^{[N]}$ can be related to the standard parameter Ω_1 relevant for $N > 1$. Our analytic predictions are tested against the hadronization model in PYTHIA, finding good agreement. The results presented in this paper demonstrate the significant advancements enabled through our new parametrization of energy correlators.

Keywords: Energy Correlators, Jet Substructure, Quantum Chromodynamics

Contents

1	Introduction	1
2	New approach to PENCs	4
3	PENCs in the back-to-back limit	7
3.1	Kinematics of PENCs in the back-to-back limit	7
3.2	Factorization in the back-to-back limit	9
3.3	One-loop jet function for PENC	11
4	Non-perturbative effects in PENC distributions	14
4.1	Structure of leading non-perturbative power corrections	15
4.2	Assessing non-perturbative corrections using PYTHIA	17
5	Conclusions	23

1 Introduction

Energy correlators have emerged as powerful tools for understanding the underlying energy flow in particle collision experiments, providing unique insights into both the perturbative and non-perturbative aspects of strong interactions [1–3]. Originally introduced in the 1970s as clean tests of perturbative quantum chromodynamics (QCD) [4–7], these observables have experienced a remarkable renaissance in recent years, driven both by the exceptional performance of modern collider detectors and significant theoretical advances in understanding their structure [8–15]. Energy correlator observables, especially the simplest two-point energy-energy correlator (EEC), have now been measured across a wide range of collision systems, from electron-positron (e^+e^-) annihilation [16, 17] to proton-proton [18–21] and heavy-ion collisions [22–24]. The ratio of the 3- and 2-point correlator has the potential to provide the most accurate α_s extraction from jet substructure measurements [18]. Precise computation of energy correlators on charged particles has also been achieved using the track function formalism, thereby enabling significant gains from the angular resolution of the tracking detectors [3, 25–29]. Beyond these, energy correlators have found numerous phenomenological applications, including the determination of the top quark mass [30–35], imaging the hadronization transition [2, 36, 37], understanding the dead-cone effect [38, 39] as well as studying jet modifications in the presence of a quark-gluon plasma [40–51].

Generalizations to higher-point correlators, though valuable for probing multi-particle correlations and for, e.g., the determination of α_s [18], become increasingly cumbersome for large values of N as they involve all $\binom{N}{2}$ pairwise distances between the N particles. While

it is simpler to study projected N -point correlators (PENCs) [14], obtained by integrating out the shape information and keeping only the largest separation between the N particles, the computational cost remains as all these distances need to be compared to determine the largest separation. The projected correlators can also be extended to non-integer N values through analytic continuation [14], which provides a novel probe of the small- x physics through jets in the $N \rightarrow 0$ limit. However, this analytic continuation scales even worse in terms of computational cost.¹ As a result, despite the interesting physics reach, the computational challenge using the traditional parametrization hindered their practical use.

In ref. [52], some of us developed a novel parametrization for N -point correlators that addresses this problem, reducing the computational cost for projected correlators to $\mathcal{O}(M^2 \ln M)$ independent of N , thus allowing for their practical utilization. Our approach reorganizes the correlator by measuring the largest angular distance with respect to a “special” particle, thereby yielding a simpler geometrical structure. Importantly, in ref. [52], we showed that, in the collinear limit, this new parametrization provides a reasonable measure of the largest angular scale and preserves the analytic properties of energy correlators. In this paper, we will utilize this approach to study the non-perturbative corrections in the collinear regime and extend our analysis to the complementary back-to-back regime.

The back-to-back limit of the EEC has been explored in the literature and analytic computations using the framework of soft collinear effective theory (SCET) [53–56] have reached the state-of-the-art accuracy of next-to-next-to-next-to-next-to-leading-logarithmic ($N^4\text{LL}$) resummation [57] including also for track-based EECs [29]. Contrary to the collinear region, where only single logarithms of the angles appear, in the back-to-back regime, the observable receives double logarithmic (Sudakov) contributions due to the presence of soft and collinear radiation. Although the explicit energy weights still suppress the contribution of the soft radiation to the measured value of EEC at leading power, the soft radiation does contribute but only through a net recoil of the energetic jets. This simplicity allows the use of the well developed theoretical framework of q_T resummation [58, 59] to obtain precise predictions for EEC in the back-to-back regime [29, 57, 60–67]. However, the extension to higher-point PENC distributions has so far not been explored.² Such computations become highly complicated already for $N = 4$ due to the complex phase-space structure for evaluating the projection.

In this work, we develop the resummation framework for higher-point PENC distributions in the back-to-back region, providing all ingredients needed at next-to-next-to-leading-logarithmic (NNLL) accuracy. We will show how the simple phase-space appearing in our approach simplifies this framework. Our work is also motivated by phenomenological considerations: First, the recent analysis of PENCs in the collinear limit, by the CMS collaboration has provided the most precise estimation of α_s from jet substructure measurements [18]. This analysis is constructed by considering the ratio of PE3C/EEC distributions which improves the precision of α_s determination by suppressing major sources of systematics, though non-perturbative effects seem to be underestimated [37]. A similar

¹Indeed, in the original paper [14] only final states with up to four particles were considered.

²For the top quark case, factorization for the three-point correlator in the back-to-back region was explored in [68].

analysis in the back-to-back regime would complement this, reducing the dominant systematics, removing for example the relative fraction of quark- to gluon-jets that affects the collinear regime [69].

We derive the factorization formula for general PENC distributions within the framework of SCET, which in the back-to-back limit takes the canonical form as for any di-jet observable. This involves a hard function encoding the short-distance dynamics of the hard scattering, jet functions describing collinear radiation within each jet and encoding the measurement of PENCs, and a soft function capturing wide-angle soft emissions. Importantly, for the EEC observable and in general for PENCs, also for our new parametrization, the explicit energy weights ensure that soft radiation contributes only to the recoil between the collinear jets, in contrast to standard di-jet observables.³ Due to our new parametrization of PENCs, only one jet function is modified compared to the EEC ($N = 2$) case. An important technical achievement of this work is then the calculation of this jet function at one-loop for arbitrary N , which was the only missing ingredient to achieve the desired NNLL accuracy⁴ for general PENCs. The anomalous dimension of this jet function was already fixed by consistency to be equal to that of q_T dependent observables.

Next, we also utilize our approach to study the leading non-perturbative power corrections to arbitrary PENC distributions in the collinear regime. The direct contribution from soft radiation to the energy correlator is power-suppressed, but needs to be taken into account when considering the non-perturbative power corrections [36, 37, 74, 75]. Furthermore, as highlighted in ref. [37] for (integer) PENC distributions, these non-perturbative contributions play an important role in the phenomenological α_s determinations. In this study, we generalize the arguments presented in refs. [37, 74] to explore the effect of power corrections for general PENC distributions, characterizing their dependence on N , the center-of-mass energy and the angular distance. Employing our new parametrization, we find that the leading non-perturbative contributions are enhanced when $N \rightarrow 0$ up to the point that the non-perturbative corrections are no longer suppressed in angular scale compared to the perturbative contribution. They also have qualitatively different behavior, e.g., the power corrections no longer scale linearly with N [75].

For $N > 1$, it was recently shown [37, 74] that leading non-perturbative effects are captured by the parameter Ω_1 [76–78]. For $N < 1$, we find a new non-perturbative matrix element, that however can be related to Ω_1 assuming it is dominated by a single non-perturbative gluon. Our estimates of the power corrections are compared to the default hadronization model used in PYTHIA simulations [79], finding good agreement with our analytic estimates.

The rest of the article is organized as follows: In sec. 2, we review the new parametrization we developed in ref. [52] and extend it for the case of back-to-back jets in e^+e^- collisions. Here, we also show the PE3C, comparing the traditional parametrization to our new

³For standard di-jet observables, soft radiation directly contributes to the measurement. If, in addition, it also contributes to the recoil of the collinear partons, this significantly complicates the perturbative calculations. For instance, computations of jet broadening and in general, recoil-sensitive angularities are particularly challenging. The presence of recoil complicates the phase-space structure of radiation already at the next-to-leading-logarithmic order [70–72].

⁴For an overview of the ingredients needed at different resummation orders, see e.g. ref. [73].

approach, using di-jet samples simulated by PYTHIA. In sec. 3, we derive the factorization theorem for PENCs in this regime and provide analytic results for the new one-loop jet function, showing explicitly the effect played by recoil on the computation of the jet function. In sec. 4, we investigate the size of leading non-perturbative contributions for PENCs and provide tests of our predictions against Monte Carlo simulations. We summarize in sec. 5.

2 New approach to PENCs

In the traditional parametrization of the projected N -point correlator, the shape information of the N -points is integrated out, keeping only the largest distance (angular separation) between all pairs of particles [14]. In ref. [52], some of us introduced a new parametrization that leads to a simpler phase-space structure, while maintaining the key physics properties in the collinear limit. There we showed that this enables a dramatic speed up, making the evaluation of the projected N -point correlator independent of N . We will recap the main points in this section and show in sec. 3 that the simpler structure has important implications for the theoretical description of the back-to-back limit. In sec. 4, we will discuss the non-perturbative corrections in the collinear limit, using this parametrization.

The key idea in our approach is to consider only the distances of all particles relative to a “special” particle i_s , and subsequently perform an energy-weighted sum over all possible choices of i_s . A cartoon illustrating the difference between the traditional parametrization and our new parametrization is shown in fig. 1.

Concretely, the N -point projected energy correlator is defined as

$$\frac{1}{\sigma} \frac{d\sigma^{[N]}}{d\chi} = \frac{1}{\sigma} \int d\sigma_X \sum_{i_s} z_{i_s} \sum_{i_1 \dots i_{N-1}} z_{i_1} \dots z_{i_{N-1}} \delta(\chi - \max_j \{\theta_{i_s, i_j}\}). \quad (2.1)$$

Here $d\sigma_X$ denotes the differential cross section for producing a hadronic final-state X , and the sums over i_s and $\{i_j\}_{j=1}^{N-1}$ run over all M particles in X , $z_i = 2E_i/Q$ are the energy fractions with respect to half the center-of-mass energy of the collision.⁵ The angular separation of particle i_j from the special particle i_s is denoted by θ_{i_s, i_j} while χ corresponds to the largest (maximum) angular separation of the $N - 1$ final-state particles i_j relative to i_s . For the special case of $N = 2$ the traditional and new parametrization coincide.

We will also use the cumulative distribution,

$$\Sigma^{[N]}(\chi) = \int_0^\chi d\chi' \frac{d\sigma^{[N]}}{d\chi'} = \int d\sigma_X \sum_{i_s=1}^M z_{i_s} [z_{\text{disk}}(i_s, \chi)]^{N-1}, \quad (2.2)$$

which provides a simple interpretation of our approach in terms of the total energy fraction $z_{\text{disk}}(i_s, \chi)$ in a disk of radius χ around the special particle i_s . This expression emphasizes that, unlike the traditional parametrization, no complications arise when generalizing to

⁵This extends the jet-based parametrization in ref. [52] to a full $e^+ e^-$ event shape. We divide by half the center-of-mass energy in z_i , as this corresponds to the jet energy in the dijet limit.

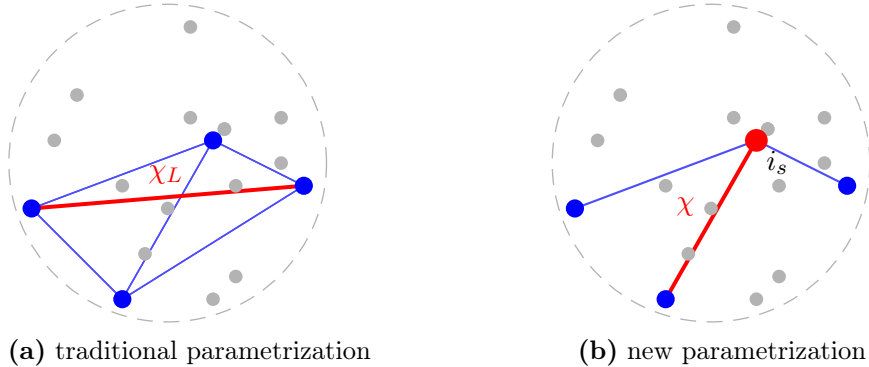


Figure 1: An illustrative diagram comparing the (a) traditional parametrization for PENCs against the (b) new parametrization for $N = 4$. In (a) all $\binom{N}{2}$ pairwise distances are needed to determine the largest separation $\chi_L = \max_{j,k} \{\theta_{i_k, i_j}\}$. By contrast, in (b) the PENCs are parametrized relative to the special particle i_s , with the largest separation characterized by $\chi = \max_j \{\theta_{i_s, i_j}\}$. In both cases all particles are summed over, including the special particle in (b). The dashed line illustrates the boundary of the jet, which is not needed in e^+e^- collisions.

non-integer values of N . It also shows that these PENCs obey the sum rule

$$\frac{1}{\sigma} \Sigma^{[N]}(\pi) = 2^N, \quad (2.3)$$

which follows directly from energy conservation as $z_{\text{disk}}(i_s, \pi) = 2$, and the summing over all possible choices of the special particle also gives $\sum_{i_s} z_{i_s} = 2$.

The cumulative distribution in eq. (2.2) allows us to highlight the major computational advantage of this new parametrization in reducing the scaling in time of the N -point projected correlator for M particles from $\mathcal{O}(M^N)$ to a simple $\mathcal{O}(M^2 \ln M)$ scaling, independent of the value of N . One factor of M arises from the sum over i_s , while the $M \ln M$ comes from sorting the particles by their distance relative to i_s , as explained in ref. [52].

On the theoretical side, this new parametrization has the same scaling behavior in the collinear limit, $\chi \rightarrow 0$, as the traditional parametrization. In the perturbative region it is given by

$$\frac{d\sigma^{[N]}}{d\chi} \sim \chi^{\gamma(N+1)-1}, \quad (2.4)$$

with differences with the traditional parametrization starting at next-to-next-to-leading logarithmic (NNLL) accuracy [52]. This translates to percent-level differences in the perturbative scaling regime for $N = 3$, as shown in the comparison between our parametrization and the traditional parametrization in fig. 2, using simulated e^+e^- collisions generated with PYTHIA 8.3 at $Q = 1$ TeV [79].

The scaling in eq. (2.4) is governed by the anomalous dimensions of the underlying theory $\gamma(N+1)$ [14], which can be expressed as the N th-moment of the time-like splitting functions $P(x)$.⁶ In the deeply non-perturbative region of the collinear limit the scaling is

⁶Technically, it should be the eigenvalues of these matrices, as the splitting functions include mixing

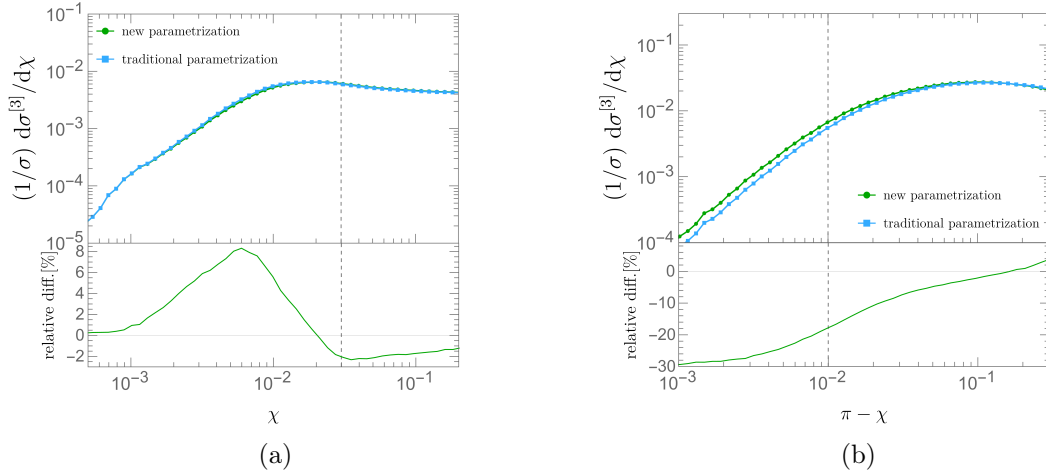


Figure 2: The PE3C distribution in $e^+ e^- \rightarrow \text{jets}$, obtained from PYTHIA at $Q = 1$ TeV, for the traditional parametrization and our new parametrization logarithmic in (a) χ and (b) $\pi - \chi$. The relative difference is shown in the bottom panel of the figure. The vertical dashed line indicates the transition between the perturbative and non-perturbative region, and the plot range is chosen to highlight the collinear region in (a) and the back-to-back regime in (b). As visible from the figure, the differences in the perturbative region are relatively small: for (a) a few percent and up to about 10% for (b), while difference in the transition to the non-perturbative region are larger but below 10% in (a) and up to 30% in (b). The larger differences for the back-to-back regime are explained in the text.

the same for the traditional and new parametrization, and corresponds to a free hadron gas. The largest differences arise in the less-understood transition region between perturbative and non-perturbative scaling, which for $N = 3$ are $\lesssim 10\%$, see fig. 2(a).

In the derivation of eq. (2.4), the inequality $\chi \leq \chi_L \leq 2\chi$ plays an important role, where χ_L would be the corresponding angle for the traditional parametrization [52]. Roughly speaking, in the collinear limit the logarithm of χ is the natural variable, due to the power-law scaling, and the difference of at most a factor of 2 does not affect that scaling. However, in the fixed-order (or bulk) region between the collinear and back-to-back limits, where there is no power-law scaling, this difference of up to a factor of 2 is relevant, leading to larger differences between the energy correlator for the traditional and new parametrization.

In the next section we will focus on the back-to-back limit, $\chi \rightarrow \pi$, deriving the factorization. In this limit the cross section contains double logarithms of $\pi - \chi$, because it becomes sensitive to the recoil of soft radiation [29, 57, 60–67]. Though we will also reach the conclusions that in this limit the differences between the traditional and new parametrization start at NNLL, numerically these differences will be much larger because the cross section contains double instead of single logarithms. Indeed, for $N = 3$ we find differences of up to 10% in the perturbative back-to-back region, as shown in fig. 2(b), while differences in the perturbative collinear region still remain at the few percent level.

Importantly, the simpler phase-space structure resulting from the new parametrization

between quarks and gluons.

makes it straightforward to generalize the theoretical description of the 2-point correlator to the projected N -point correlator in the yet unexplored back-to-back limit, and we will provide the ingredients necessary for NNLL resummation.

3 PENCs in the back-to-back limit

In this section, we provide analytic results for the new PENCs in the back-to-back limit. We start by discussing in detail the kinematics of PENCs in sec. 3.1, and present the factorization in this regime in sec. 3.2. We provide explicit one-loop results for the new jet function in sec. 3.3, which is the only extra ingredient needed to achieve NNLL accuracy.

3.1 Kinematics of PENCs in the back-to-back limit

The structure of the two-point energy correlator has been investigated extensively in the literature in the back-to-back region [29, 57, 60–67]. Here, we briefly review it, allowing us to introduce the necessary concepts and notation, after which we extend to PENCs with general N .

For e^+e^- collisions, it is convenient to use

$$x = \frac{1 - \cos \chi}{2}. \quad (3.1)$$

instead of the angle χ , such that the back-to-back limit $\chi \rightarrow \pi$ corresponds to $x \rightarrow 1$. In this limit, the event consists of two nearly back-to-back jets, which will be described by collinear radiation. The offset from exact back-to-back jets is due to both the collinear and soft radiation; with soft radiation providing a color connection between the two jets. The energy weights in the definition of the EEC (see eq. (2.1) with $N = 2$) suppress any direct contribution from soft radiation at leading power, such that its only effect is through recoil. This will no longer be the case for the sub-leading corrections due to hadronization in sec. 4.

We will use light-cone variables to parametrize the momenta of the particles in the final state. In these coordinates, any four-momentum can be decomposed as

$$p^\mu = n \cdot p \frac{\bar{n}^\mu}{2} + \bar{n} \cdot p \frac{n^\mu}{2} + \mathbf{p}^\mu = (n \cdot p, \bar{n} \cdot p, \mathbf{p}^\mu) \quad (3.2)$$

where $n = (1, 0, 0, 1)$ and $\bar{n} = (1, 0, 0, -1)$ are the light-like directions along the initial quark and anti-quark produced in the e^+e^- collision.⁷ We omit the \perp on the transverse components \mathbf{p}^μ for brevity.

In terms of the effective theory formulation, the relevant modes that contribute to the EEC in the back-to-back limit are: two collinear modes describing the energetic radiation in the two jets, and a soft mode that encodes the recoil of these jets due to the low energy

⁷While this specific frame is not experimentally accessible, it simplifies the discussion, and the final result is frame independent.

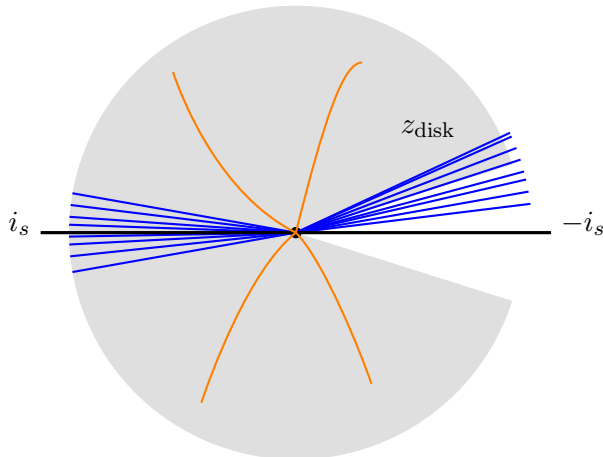


Figure 3: Schematic of the back-to-back regime, where the special particle is in one of the jets and the measurement is sensitive to details of the collinear radiation in the opposite jet, through their distance to the antipode of the special particle $-i_s$, i.e. whether these particles are included in z_{disk} shown in gray. The soft radiation produces an overall recoil, such that the jets are no longer exactly back-to-back.

radiation. These modes are described by the following scaling of their light-cone momenta,

$$\begin{aligned}
 n\text{-collinear:} & & p_n &\sim Q(1, \lambda^2, \lambda), \\
 \bar{n}\text{-collinear:} & & p_{\bar{n}} &\sim Q(\lambda^2, 1, \lambda), \\
 \text{soft:} & & p_{\text{soft}} &\sim Q(\lambda, \lambda, \lambda),
 \end{aligned} \tag{3.3}$$

in terms of the power counting parameter $\lambda \sim \sqrt{1-x} \sim \pi - \chi$ and the center-of-mass energy Q of the collision. The effective theory whose modes satisfy the power counting in eq. (3.3) is known as SCET_{II} [80]. As the recoil concerns the momentum component perpendicular to the jet, the corresponding \mathbf{p} component has the same λ -scaling for all these modes.

Indeed, the expression of the angular scale x for the n -collinear parton i and \bar{n} -collinear parton j is [63]

$$\begin{aligned}
 1 - x &= \frac{\mathbf{p}^2}{Q^2} = \frac{1}{Q^2} \left(\frac{\mathbf{p}'_i}{z_i} + \frac{\mathbf{p}'_j}{z_j} - \mathbf{p}_{\text{soft}} \right)^2 \\
 &= \frac{1}{Q^2} (\mathbf{p}_i + \mathbf{p}_j - \mathbf{p}_{\text{soft}})^2,
 \end{aligned} \tag{3.4}$$

where we have dropped power corrections. Here, $z_{i,j}$ denote the fraction of the jet energy carried by partons i and j , $\mathbf{p}'_{i,j}$ their transverse momenta with respect to the initiating parton (or field), and \mathbf{p}_{soft} is the *total* transverse momentum of soft radiation. Since only this specific ratio of the hadronic variables $\mathbf{p}'_{i,j}$ and $z_{i,j}$ appears, it is convenient to switch to their ratio, which is a partonic variable that we denote by $\mathbf{p}_{i,j}$.

For the traditional parametrization, generalizing these arguments to PENCs is non-trivial because all possible distances between subsets of particles in *both* jets are needed to compute their largest separation. In our approach, the phase-space structure is simplified because we only have to consider distances to the special particle. If the special particle is in one jet, we just have to consider the distances to subsets of particles in the other jet. Instead of the largest distance χ we can equivalently consider the smallest distance $\pi - \chi$ to the antipode of the special particle, depicted in fig. 3. This means that the complications for $N \neq 2$ reside entirely in the other jet function, while the jet containing the special particle is described by the same jet function J as for $N = 2$. Indeed, collinear emissions in the jet containing the special particle are always included in the disk of radius χ when $\chi \rightarrow \pi$, i.e. they never set the largest distance and the sum over their momentum fractions is 1.⁸

The new jet function, which we denote as J_{N-1} , takes as input the antipode of the special particle, characterized by $\mathbf{p}_{\text{ap}} = -\mathbf{p}'_s/z_s + \mathbf{p}_{\text{soft}} = -\mathbf{p}_s + \mathbf{p}_{\text{soft}}$ where s labels the special particle (which is not soft). The term \mathbf{p}_{soft} accounts for the recoil from soft radiation. This complicates the factorization structure compared to the simpler additive structure in eq. (3.4), where the jet function's contributions to the distance x can be calculated independently of each other. Because the jet is insensitive to the initiating quark spin at leading power, the jet function J_{N-1} has azimuthal symmetry, it can only depend on the *relative* angle ϕ between its contribution to the transverse momentum \mathbf{p} and \mathbf{p}_{ap} . At leading order, the jet function contains a single parton, which is automatically the one closest to the antipode, and the measurement can still be written as in (3.4).

With the knowledge of the modes that contribute in the back-to-back regime and a discussion of the observable, we are now ready to write down the factorization theorem and discuss its ingredients, in the following section.

3.2 Factorization in the back-to-back limit

The factorized cross-section for PENCs can be written as a product of the hard function H , that characterizes the hard scattering event generating the energetic back-to-back partons $e^+ e^- \rightarrow q\bar{q}$, with a convolution between the jet function J and the soft function S governing the evolution of the energetic quark and anti-quark at subsequent energy scales.⁹ In particular, the jet function J describes the dynamics of collinear radiation inside the jet, while the soft function S accounts for the low energy exchanges between the two back-to-back jets. At leading power in SCET, the interactions between the jet and soft degrees of freedom are decoupled through a BPS field redefinition [54] and only appear in the current.¹⁰ As a result, there are no interactions between collinear and soft radiation, and each of the hard, jet and soft functions describe the dynamics at a single scale. This allows the

⁸We find it convenient to use a convention in which the total momentum fraction of all collinear radiation in a jet is 1, because otherwise the number of detectors in the jet with the special particle would yield a nontrivial overall factor for the jet function.

⁹As we are considering $e^+ e^-$ collisions, we do not have to consider possible Glauber exchanges between incoming hadrons.

¹⁰Although this is strictly a SCET_I statement, it is common to match onto SCET_{II} through an intermediate SCET_I theory, which shows how Wilson lines appear.

large logarithms of $1 - x$ to be resummed through the solution of the renormalization group equations, evolving the respective functions from their natural scale to a single common scale.

In terms of these ingredients, the factorized cross-section in the back-to-back regime can be written as

$$\begin{aligned} \frac{1}{\sigma_0} \frac{d\sigma^{[N]}}{dx} &= H(Q; \mu) \int d^2\mathbf{p}_n J(\mathbf{p}_n^2; \mu, \nu) \int d^2\mathbf{p}_{\text{soft}} S(\mathbf{p}_{\text{soft}}^2; \mu, \nu) \int d^2\mathbf{p}_{\bar{n}} \\ &\times J_{N-1}(\mathbf{p}_{\bar{n}}, -\mathbf{p}_n + \mathbf{p}_{\text{soft}}; \mu, \nu) \delta\left[1 - x - \frac{1}{Q^2}(\mathbf{p}_n + \mathbf{p}_{\bar{n}} - \mathbf{p}_{\text{soft}})^2\right] + \{n \leftrightarrow \bar{n}\}. \end{aligned} \quad (3.5)$$

The measurement x of the largest distance is fixed in terms of the contributions from particles in the jet and soft sectors, described by the transverse momentum variables $\mathbf{p}_{\{n, \bar{n}, \text{soft}\}}$. Here J is the same jet function as for the EEC ($N = 2$) [63] and does not involve any N -dependence because in the back-to-back regime the particles in the jet with the special particle are always included in z_{disk} . The other jet function, describing the jet without the special particle, and containing (up to) $N - 1$ detectors, is denoted by J_{N-1} . J_{N-1} contains all multinomial factors, arising for higher-point correlators, associated with how many of the N detectors are on the jet [14, 75, 81]. Finally, μ (ν) represent the renormalization scales for (rapidity) renormalization group evolution (RGE). We will use the rapidity regulator of ref. [82], for other choices of the rapidity regulator, see e.g., refs. [83–87]. The presence of rapidity divergences and the corresponding ν -evolution is intrinsic of the fact that PENCs in the back-to-back limit are SCET_{II} observables.

The hard function H in the above equation is the same as that for any $e^+ e^- \rightarrow$ di-jet observable. At next-to-leading order (NLO), the hard function is given by [88, 89]

$$H(Q; \mu) = 1 + \frac{\alpha_s(\mu)C_F}{\pi} \left(-2 \ln^2 \frac{\mu}{Q} - 3 \ln \frac{\mu}{Q} - 4 + \frac{7}{2} \zeta_2 \right), \quad (3.6)$$

The soft function S only contributes to the observable through an overall recoil momentum \mathbf{p}_{soft} . Consequently, it remains the same as for the two-point energy correlator. The soft function has been evaluated up to three loops and the corresponding results (including the one-loop) can be found in refs. [29, 63]. The resummation is most easily carried out in the Fourier conjugate space, for which the soft function up to NLO is given by

$$S(\mathbf{b}^2; \mu, \nu) = 1 + \frac{\alpha_s(\mu)C_F}{\pi} \left[-\frac{1}{2} \ln^2 \left(\frac{\mathbf{b}^2 \mu^2 e^{2\gamma_E}}{4} \right) + \ln \left(\frac{\mathbf{b}^2 \mu^2 e^{2\gamma_E}}{4} \right) \ln \left(\frac{\mu}{\nu} \right) - 2\zeta_2 \right]. \quad (3.7)$$

Here the impact parameter \mathbf{b} is Fourier conjugate to \mathbf{p}_{soft} .

The jet function $J = J_1$, i.e. J_{N-1} with $N = 2$. Consequently, we don't discuss it separately, but leave it for the next section in which we discuss the calculation of J_{N-1} . Nevertheless, J_1 is substantially simpler, and has been obtained by taking moments of the transverse momentum dependent fragmentation functions [83, 90]. Only the jet function J_{N-1} is sensitive to the N -dependence of the measured N -point correlator. At NLL accuracy, where the resummation only requires the tree-level hard, jet, and soft functions and

the evolution is determined by their anomalous dimensions, there is no difference between the traditional and new parametrizations. In particular, the tree-level jet functions each involve a single collinear parton, for which this difference is irrelevant. As highlighted in the previous section, the simplicity of our approach allows us to generalize the computation to any arbitrary PENC without the requirement of additional phase-space considerations.

3.3 One-loop jet function for PENC

We now compute the new jet function J_{N-1} for the jet not containing the special particle, at one-loop accuracy. This contains all non-trivial N -dependence. As previously stated, the jet function J with the special particle is equal to the jet function for the two-point energy correlator, $J = J_1$.

The jet function can be computed from the QCD splitting functions, as was shown at NNLO in ref. [91]. This averts the use of the more complicated collinear Feynman rules in SCET. Writing the (bare) jet function in terms of a collinear phase-space integral over the P_{qq} QCD splitting function,¹¹

$$J_{N-1}(\mathbf{p}, \mathbf{p}_{\text{ap}}; \mu, \nu) = \frac{\alpha_s C_F}{2\pi^2} \frac{e^{\epsilon\gamma_E} \mu^{2\epsilon}}{\Gamma(1-\epsilon)} \left(\frac{\nu}{Q}\right)^\eta \int \frac{dz}{(1-z)^\eta} \int \frac{d^2\mathbf{k}}{(\mathbf{k}^2)^{1+\epsilon}} P_{qq}(z) \mathcal{O}_{N-1}(\mathbf{p}, \mathbf{p}_{\text{ap}}, z, \mathbf{k}),$$

$$P_{qq}(z) = \frac{1+z^2}{1-z} - \epsilon(1-z). \quad (3.8)$$

Here ϵ (η) is the dimensional (rapidity) regulator, with the associated (rapidity) renormalization scale denoted by μ (ν). The strong coupling is denoted by α_s , and $C_F = 4/3$ is the color factor for quark-initiated jets. Finally, \mathcal{O} encodes the measurement, which in the absence of recoil $\mathbf{p}_{\text{ap}} = \mathbf{0}$ is given by

$$\mathcal{O}_{N-1}(\mathbf{p}, \mathbf{0}, z, \mathbf{k}) = \Theta\left(z < \frac{1}{2}\right) \left\{ [(1+z)^{N-1} - 1^{N-1}] \delta^2\left(\mathbf{p} - \frac{\mathbf{k}}{z}\right) + [2^{N-1} - (1+z)^{N-1}] \delta^2\left(\mathbf{p} + \frac{\mathbf{k}}{1-z}\right) \right\} + (z \leftrightarrow 1-z). \quad (3.9)$$

The Θ -function encodes that if $z < \frac{1}{2}$, the particle with momentum fraction $1-z$ is closer to the antipodal point and therefore gets added later to z_{disk} . The change in z_{disk} , shown in square brackets, contributes at the distance of the corresponding emission, encoded in \mathbf{p} . Performing the z and \mathbf{k} integral, renormalizing the expression, and including the tree-level result

$$J_{N-1}(\mathbf{p}, \mathbf{0}; \mu, \nu) = (2^{N-1} - 1) \left(\delta^2(\mathbf{p}) + \frac{\alpha_s C_F}{\pi} \left\{ j_{N-1} \delta^2(\mathbf{p}) + \left[2 \ln\left(\frac{Q}{\nu}\right) - \frac{3}{2} \right] \mathcal{L}_0^T(\mathbf{p}, \mu) \right\} \right), \quad (3.10)$$

where we find it convenient to pull out the tree-level coefficient $2^{N-1} - 1$ and \mathcal{L}_0^T is the plus

¹¹Technically, dimensional regularization yields a $(\sin \phi')^{-2\epsilon}$ dependence on the angle ϕ' of \mathbf{k} in the transverse plane. In our case this does not affect the result.

distribution defined through

$$\mathcal{L}_n^T(\mathbf{p}, \mu) = \frac{1}{2\pi\mu^2} \left[\frac{\ln^n(\mathbf{p}^2/\mu^2)}{\mathbf{p}^2/\mu^2} \right]_+ . \quad (3.11)$$

The general form for the coefficient j_{N-1} of $\delta^2(\mathbf{p})$ is

$$j_{N-1} = \frac{1}{2^{N-1}-1} \int dz \left(\frac{2^{N-1}-1}{2} (1-z) + \frac{1+z^2}{1-z} \left\{ \left[((1+z)^{N-1}-1) \ln z + (2^{N-1} - (1+z)^{N-1}) \ln(1-z) \right] \Theta(z < 1/2) + (z \leftrightarrow 1-z) \right\} \right), \quad (3.12)$$

which for specific values of N results in

$$j_{-0.5} = -3.04, \quad j_1 = 1 - 2\zeta_2, \quad j_2 = \frac{25}{24} + \frac{1}{2} \ln 2 - 2\zeta_2, \quad j_3 = \frac{57}{56} + \frac{27}{28} \ln 2 - 2\zeta_2. \quad (3.13)$$

We now move on to the case of recoil, which we write as

$$J_{N-1}(\mathbf{p}, \mathbf{p}_{\text{ap}}; \mu, \nu) = J_{N-1}(\mathbf{p}, \mathbf{0}; \mu, \nu) + \Delta J_{N-1}(\mathbf{p}, \mathbf{p}_{\text{ap}}; \mu, \nu). \quad (3.14)$$

The expression for ΔJ is the same as eq. (3.8), with the measurement \mathcal{O} replace by $\Delta\mathcal{O}$, given in eq. (3.20) below. Moreover, as the recoil correction is finite, there is no dependence on the scales μ, ν in ΔJ at this order. Compared to the case without recoil, the boundary is no longer simply at $z = \frac{1}{2}$ but follows from

$$\left| \frac{\mathbf{k}}{z} - \mathbf{p}_{\text{ap}} \right| = \left| \frac{\mathbf{k}}{1-z} + \mathbf{p}_{\text{ap}} \right|, \quad (3.15)$$

which has as solution

$$z'_* = \frac{1}{2} + \frac{|\mathbf{k}| - \sqrt{\mathbf{k}^2 + \mathbf{p}_{\text{ap}}^2 \cos^2 \phi'}}{2|\mathbf{p}_{\text{ap}}| \cos \phi'}, \quad (3.16)$$

where ϕ' is the angle between \mathbf{k} and \mathbf{p}_{ap} . For $0 < \phi' < \frac{\pi}{2}$ this satisfies $z'_* < \frac{1}{2}$, while for $\frac{\pi}{2} < \phi' < \pi$ instead $z'_* > \frac{1}{2}$.

However, this form is not so convenient, because there is a delta function that will cause \mathbf{k} to be replaced by $z\mathbf{p}$ or $-(1-z)\mathbf{p}$. To determine the boundary in terms of \mathbf{p} , we consider these two cases separately,

$$z_* = \begin{cases} \frac{1}{2} - \frac{|\mathbf{p}_{\text{ap}}| \cos \phi}{2(|\mathbf{p}| - |\mathbf{p}_{\text{ap}}| \cos \phi)} & \cos \phi < \frac{|\mathbf{p}|}{2|\mathbf{p}_{\text{ap}}|}, \\ 0 & \cos \phi > \frac{|\mathbf{p}|}{2|\mathbf{p}_{\text{ap}}|}, \end{cases} \quad (3.17)$$

where z_* (or equivalently, $1-z_*$) corresponds to the case where the particle with momentum fraction z (or, $1-z$) sets \mathbf{p} . Note that ϕ now denotes the angle between \mathbf{p} and \mathbf{p}_{ap} , though again $z_* < \frac{1}{2}$ for $0 < \phi < \frac{\pi}{2}$ and $z_* > \frac{1}{2}$ for $\frac{\pi}{2} < \phi < \pi$. We thus need to correct the

no-recoil measurement as follows

$$\begin{aligned} \Delta\mathcal{O}_{N-1}(\mathbf{p}, \mathbf{p}_{\text{ap}}, z, \mathbf{k}) &= \left\{ [2^{N-1} - (2-z)^{N-1}] - [(1+z)^{N-1} - 1^{N-1}] \right\} \\ &\times \left[\Theta\left(z_* < z < \frac{1}{2}\right) - \Theta\left(\frac{1}{2} < z < z_*\right) \right] \delta^2\left(\mathbf{p} - \frac{\mathbf{k}}{z}\right) + (z \leftrightarrow 1-z). \end{aligned} \quad (3.18)$$

Note that for $N = 2$, $\Delta\mathcal{O}_1 = 0$ and thus $\Delta J_1 = 0$, as expected. The $1/(1-z)$ soft divergence of the splitting function will be regulated by this measurement, because $z_* < 1$, while when $z_* = 0$ (for the $z \leftrightarrow 1-z$ term)

$$[2^{N-1} - (2-z)^{N-1}] - [(1+z)^{N-1} - 1] = \mathcal{O}(z), \quad (3.19)$$

thus taming the singularity.

For general N , this leads to a finite correction ΔJ_{N-1} , which can be written as¹²

$$\begin{aligned} \Delta J_{N-1}(|\mathbf{p}|, |\mathbf{p}_{\text{ap}}|, \phi) &= \frac{\alpha_s C_F}{\pi} \left[\int d^2\mathbf{k} dz \mathcal{L}_0^T(\mathbf{k}, \mu) \frac{1+z^2}{1-z} \Delta\mathcal{O}_{N-1}(\mathbf{p}, \mathbf{p}_{\text{ap}}, z, \mathbf{k}) \right. \\ &\quad \left. + \delta^2(\mathbf{p}) \int dz \frac{1+z^2}{1-z} \ln z \Delta\mathcal{O}_{N-1}(\mathbf{0}, \mathbf{p}_{\text{ap}}, z, \mathbf{0}) \right] \\ &= (2^{N-1} - 1) \frac{\alpha_s C_F}{\pi} \left[\mathcal{L}_0^T(\mathbf{p}, \mu) \Delta\mathcal{F}_{N-1}(|\mathbf{p}|, |\mathbf{p}_{\text{ap}}|, \phi) + \delta^2(\mathbf{p}) \Delta j_{N-1} \right], \end{aligned} \quad (3.20)$$

again pulling out the tree-level factor $(2^{N-1} - 1)$. The coefficients $\Delta\mathcal{F}_{N-1}$ and Δj_{N-1} are defined through the integrals

$$\begin{aligned} \Delta\mathcal{F}_{N-1} &= \frac{1}{2^{N-1} - 1} \int dz \left(\frac{1+z^2}{1-z} + (z \leftrightarrow 1-z) \right) \left\{ [2^{N-1} - (2-z)^{N-1}] \right. \\ &\quad \left. - [(1+z)^{N-1} - 1] \right\} \left[\Theta\left(z_* < z < \frac{1}{2}\right) - \Theta\left(\frac{1}{2} < z < z_*\right) \right], \end{aligned} \quad (3.21)$$

$$\begin{aligned} \Delta j_{N-1} &= \frac{1}{2^{N-1} - 1} \int \frac{d\phi}{\pi} \int dz \left(\frac{1+z^2}{1-z} + (z \leftrightarrow 1-z) \right) \ln z \left\{ [2^{N-1} - (2-z)^{N-1}] \right. \\ &\quad \left. - [(1+z)^{N-1} - 1] \right\} \left[\Theta\left(z_* < z < \frac{1}{2}\right) - \Theta\left(\frac{1}{2} < z < z_*\right) \right] \Big|_{|\mathbf{p}|=0}, \end{aligned} \quad (3.22)$$

where the symmetrization $z \leftrightarrow 1-z$ has been moved to the splitting functions, for simplicity. The dependence of $\Delta\mathcal{F}_{N-1}$ on $|\mathbf{p}_{\text{ap}}|$ and ϕ is hiding in z_* . By contrast, Δj_{N-1} does not depend on these because it is evaluated at $|\mathbf{p}| = 0$. In principle it has a dependence on ϕ , because

$$z_* \Big|_{|\mathbf{p}| \rightarrow 0} \begin{cases} 0 & 0 < \phi < \frac{\pi}{2}, \\ 1 & \frac{\pi}{2} < \phi < \pi, \end{cases} \quad (3.23)$$

as in this limit which particle is closest to the antipode only depends on ϕ . However, at $|\mathbf{p}| = 0$ this angle becomes ill-defined, which is why we average over it in (3.22). This

¹²While the expression contains explicit μ -dependence, this dependence cancels in the final result.

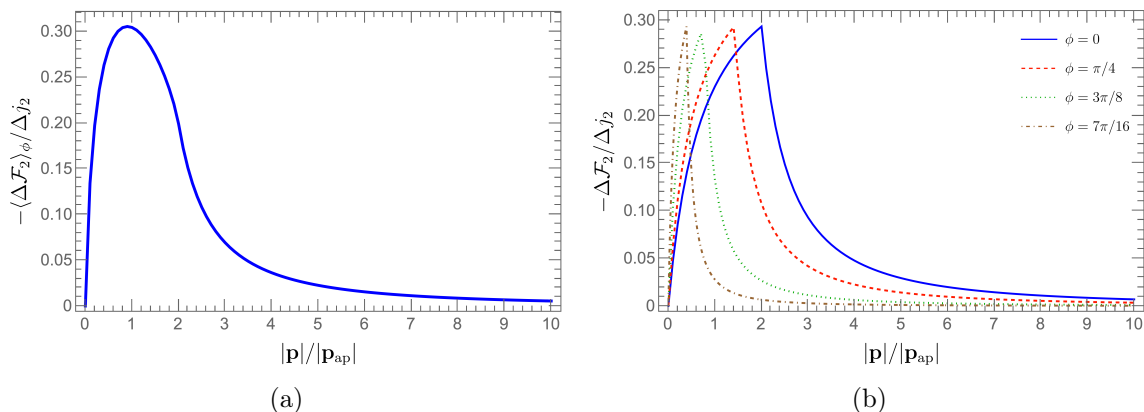


Figure 4: Coefficient $\Delta\mathcal{F}_{N-1}$ of the plus-distribution due to recoil in (3.20) for $N = 3$, (a) averaged over ϕ and (b) for specific ϕ values. The N -dependence is largely an overall factor.

results in¹³

$$\Delta j_{-0.5} = 0.621, \quad \Delta j_1 = 0, \quad \Delta j_2 = -\frac{1}{24} - \frac{1}{2} \ln 2, \quad \Delta j_3 = -\frac{9}{112} - \frac{27}{28} \ln 2. \quad (3.24)$$

The remaining coefficient $\Delta\mathcal{F}_{N-1}$ of the plus-distribution in eq. (3.20) is plotted in fig. 4 as function of $|\mathbf{p}|/|\mathbf{p}_{\text{ap}}|$ both for specific values of ϕ and averaged over ϕ (indicated by $\langle \dots \rangle_\phi$). In the ϕ dependent result there is a qualitative change due to the distinct cases in (3.17), which gets washed out when averaging over ϕ . We only show the result for $N = 3$, as we have verified for a range of values of N (including $N = 0.5$) that $\Delta\mathcal{F}_{N-1}/\Delta j_{N-1}$ is largely independent of N , up to corrections of a few percent. At the same time, we emphasize that $\Delta j_{N-1}/j_{N-1}$ changes with N .

4 Non-perturbative effects in PENC distributions

Although PENCs obey simple scaling laws in perturbation theory, the non-perturbative power corrections can be sizable. For the two-point energy correlator, refs. [78, 92] demonstrated that leading corrections of order $\mathcal{O}(\Lambda_{\text{QCD}}/Q)$ contribute across the entire range of angular scales, rather than being confined to the collinear and back-to-back region. In recent years, considerable effort has been devoted to understanding the size and structure of these leading $\mathcal{O}(\Lambda_{\text{QCD}}/Q)$ corrections for EEC observables, employing both renormalon-based approaches as well as light-ray operator product expansion techniques [36, 37, 74].

These approaches have been extended to (integer) PENCs in [36, 37], while the expected Λ_{QCD}/Q structure of the analytically continued (non-integer) PENCs was first discussed in [75]. In particular, ref. [75] highlighted that for $N < 1$ non-perturbative corrections become increasingly important and the leading corrections are no longer linear in Λ_{QCD}/Q . In

¹³We can also directly calculate $\Delta\mathcal{F}_{N-1}$ analytically in the $\mathbf{p} \rightarrow 0$ limit, which resulted in these analytical results for Δj_{N-1} and provided us with a check. It also showed that $\Delta\mathcal{F}_{N-1} \rightarrow 0$ in this limit.

this study, we: (1) use our new parametrization¹⁴, which allows for a realistic computation of (non-integer) PENCs with equal ease [52], (2) predict how the leading power-corrections depend on both the angular scale x and the value of N and (3) test this dependence across PENCs through the use of Monte Carlo simulations.

Before discussing non-perturbative power corrections to PENCs, we would like to state an important caveat that caused us to limit our analysis to the collinear regime. In the traditional formulation, non-perturbative corrections to back-to-back configurations only impact the back-to-back region, i.e., $\chi \rightarrow \pi \sim \theta_{c_1, c_2}$, with $c_{1,2}$ representing collinear particles along the two different collinear directions in the back-to-back region. However, for our parametrization, depending on whether the special particle (s) is placed on the collinear particle $s \in c_{1,2}$ or a wide-angled soft particle $s \in \text{soft}_{\text{NP}}$, two contributions arise. When the special particle is a collinear particle, the leading non-perturbative contributions with a single non-perturbative gluon still contribute to the $\chi \sim \pi$ angular regime. On the contrary, if the special particle is the non-perturbative gluon itself, these contributions now migrate to the fixed-order regime as $\theta_{s, c_1/c_2} < \theta_{c_1, c_2} \sim \pi$. Therefore, sizable modifications due to non-perturbative effects can arise in the fixed-order region of the correlator, which we observe in PYTHIA. Consequently, we choose to focus only on the collinear regime for the rest of our discussion.

In the next section, we begin by discussing the leading order structure of the power corrections for any N -point energy correlator, and in sec. 4.2 we test our analytic predictions against the hadronization model used in the PYTHIA Monte Carlo simulation [79].

4.1 Structure of leading non-perturbative power corrections

The leading power correction to N -point energy correlators can be schematically written as [36, 37, 74, 78, 92]

$$\frac{1}{\sigma} \frac{d\sigma^{[N]}}{dx} = \frac{1}{\sigma} \frac{d\hat{\sigma}^{[N]}}{dx} + \text{power corrections}, \quad (4.1)$$

where $\sigma^{[N]}$ denotes the full PENC distribution including non-perturbative effects, while $\hat{\sigma}^{[N]}$ represents the perturbative contribution. Though power corrections are relevant across the whole angular regime for energy correlators, their analytic structure turns out to be significantly simpler compared to standard di-jet observables.

Indeed, ref. [74] showed that employing the same leading power-correction parameter, Ω_1 , extracted from thrust data in the di-jet limit of e^+e^- collisions [93] yields an excellent description of the EEC distribution in the existing e^+e^- collider data [94–96]. This agreement holds across most of the measured phase space without requiring additional fits, with deviations appearing only near the kinematic endpoints where higher-order effects become important. The leading non-perturbative correction entering these analyses is obtained by performing a non-perturbative operator product expansion [97, 98], resulting in a calculable

¹⁴The computation of (non-integer) PENCs in ref. [75] relies on an approximate approach that uses sub-jets instead of final-state particles [81].

coefficient and a non-perturbative matrix element Ω_1 of soft Wilson lines, $Y_n, Y_{\bar{n}}$

$$\Omega_{1,k} = \frac{1}{N_k} \langle 0 | \bar{Y}_{\bar{n}}^{\dagger k} Y_n^{\dagger k} \mathcal{E}_T(0) Y_n^k \bar{Y}_{\bar{n}}^k | 0 \rangle, \quad (4.2)$$

where $k = q, g$ denotes the color channel (corresponding to the fundamental or adjoint representation for the Wilson lines) and $N_q = N_c$, $N_g = N_c^2 - 1$ [99, 100]. Here \mathcal{E}_T is the boost-invariant transverse energy flow operator, which is related to the longitudinal energy flow operator as [98]

$$\mathcal{E}_T = \frac{\mathcal{E}(\eta)}{\cosh \eta}. \quad (4.3)$$

Employing similar arguments as in ref. [37], we now derive the leading power corrections for general N within our parametrization.

The leading non-perturbative correction arises when a single non-perturbative gluon is correlated with the collinear particles in the jet. For simplicity, consider a single collinear particle described by momentum fraction z_c and a non-perturbative gluon carrying momentum fraction z_{NP} , with $z_{\text{NP}} \sim \mathcal{O}(\Lambda_{\text{QCD}}/Q)$.¹⁵ The contribution to the (differential) energy correlator from a collinear particle and a non-perturbative gluon then gives

$$\left\{ z_c [(z_c + z_{\text{NP}})^{N-1} - z_c^{N-1}] + z_{\text{NP}} [(z_c + z_{\text{NP}})^{N-1} - z_{\text{NP}}^{N-1}] \right\} \delta(\chi - \theta_{\text{NP},c}), \quad (4.4)$$

where $\theta_{\text{NP},c}$ is the angle between the collinear particle and the non-perturbative gluon. In the first term, the special particle is the collinear particle while in the second the special particle is the non-perturbative gluon.

Expanding the two terms, keeping only the leading terms in z_{NP} gives

$$\left\{ (N-1) z_c^{N-1} z_{\text{NP}} + z_{\text{NP}} [z_c^{N-1} - z_{\text{NP}}^{N-1}] \right\} \delta(\chi - \theta_{\text{NP},c}). \quad (4.5)$$

The two $z_{\text{NP}} z_c^{N-1}$ terms combine to produce the familiar leading non-perturbative corrections that grow linearly with N , similar to the result for (integer) $N \geq 2$ studied in the literature [36, 37]. The extra term proportional to z_{NP}^N is suppressed when $N > 1$ but provides the dominant contribution for $N < 1$. As a result, the leading non-perturbative power corrections have a qualitatively different structure for $N < 1$ than for $N > 1$. Importantly, the result in eq. (4.5) predicts that the non-perturbative corrections are *negative* for $N < 1$. In sec. 4.2, we will also find that this negative sign appears in the Monte Carlo simulations.

Rewriting η in terms of the angle χ and then expressing that in terms of x using eq. (3.1) results in

$$\cosh \eta = \frac{1}{2\sqrt{x(1-x)}} \sim \frac{1}{2\sqrt{x}}, \quad (4.6)$$

in the collinear limit. We use this to rewrite the energy flow in terms of the boost-

¹⁵Technically, adding more collinear particles for the description of the leading non-perturbative effect, dictated by a single non-perturbative gluon, is straightforward as long as their relative angle is small compared to the angle with the non-perturbative gluon. However, to keep the expressions simple we focus on only a single collinear particle.

invariant transverse energy flow operator, arriving at the following form for the leading non-perturbative corrections at leading order in α_s ¹⁶

$$\begin{aligned} \frac{1}{\sigma} \frac{d\sigma_{\text{NP}}^{[N]}}{dx} &\equiv \frac{1}{\sigma} \frac{d\sigma^{[N]}}{dx} - \frac{1}{\sigma} \frac{d\hat{\sigma}^{[N]}}{dx}, \\ &= \frac{N \Omega_1}{2^N Q x^{3/2}} - \frac{\tilde{\Omega}^{[N]}}{2^N Q x^{1+N/2}}. \end{aligned} \quad (4.7)$$

Here $d\sigma_{\text{NP}}$ is the difference of the full PENC distribution and the perturbative computation and x , defined in eq. (3.1), is roughly $\chi^2/4$ in the collinear limit. We have additionally replaced the momentum fraction of the non-perturbative gluon with the parameter Ω_1 (see eq. (4.2)) and the parameter $\tilde{\Omega}^{[N]}$ (discussed below). The factor of $1/2^N$ in the above equation arises due to normalization: we simulate $e^+ e^- \rightarrow q\bar{q}$ events and hence the overall energy weights involved in the definition of PENC contain a factor of $Q/2$ for each particle. The factor of $1/2^N$ therefore ensures that the sum rule evaluates to 1.

For $N < 1$, we find a new non-perturbative matrix element, which we denote as $\tilde{\Omega}^{[N]}$, that can be expressed as the matrix element of soft Wilson lines containing N powers of energy flow operators as

$$\tilde{\Omega}^{[N]} = \frac{1}{N_k} \langle 0 | \bar{Y}_n^{\dagger k} Y_n^{\dagger k} \mathcal{E}_T^N(0) Y_n^k \bar{Y}_n^k | 0 \rangle, \quad (4.8)$$

We will discuss $\tilde{\Omega}^{[N]}$ in more detail in the next section. Due to the presence of N powers of the non-perturbative gluon, for $N < 1$, the dependence on the angular scale x becomes non-trivial going as $x^{-1-N/2}$, where the x^{-1} is just the classical scaling for differential energy correlators, see eq. (2.4). Importantly, this implies that the non-perturbative power corrections approach the same classical scaling in x as the perturbative term for $N \rightarrow 0$.

4.2 Assessing non-perturbative corrections using PYTHIA

We simulate electron-positron (e^+e^-) annihilation events using the PYTHIA 8.3 Monte Carlo event generator, considering the process $e^+e^- \rightarrow \text{jets}$ at $Q = 1 \text{ TeV}$. The choice of Q ensures a large collinear region of the distribution where our predictions for the non-perturbative contributions can be tested. Specifically, we want a sufficiently large region where the collinear factorization holds, while at the same time only including the leading non-perturbative corrections suffices. A total of 10^6 events were used to compute the PENC distributions from the simulated data. In addition, to study the dependence of the power corrections on the center-of-mass energy, we also generated events at $Q = 500 \text{ GeV}$.

To determine the size of non-perturbative corrections in the simulations, we generate event samples both with and without hadronization effects enabled. The estimate of non-perturbative contributions from the Monte Carlo simulated data is then taken to be

$$\frac{1}{\sigma} \frac{d\sigma_{\text{NP,MC}}^{[N]}}{dx} = \frac{1}{\sigma} \frac{d\sigma_{\text{hadron}}^{[N]}}{dx} - \frac{1}{\sigma} \frac{d\sigma_{\text{parton}}^{[N]}}{dx}, \quad (4.9)$$

¹⁶Interestingly, a similar dependence of the non-perturbative contributions on Λ_{QCD}/Q was observed for jet angularities in ref. [101]. The connection of their findings to our results merits further investigation.

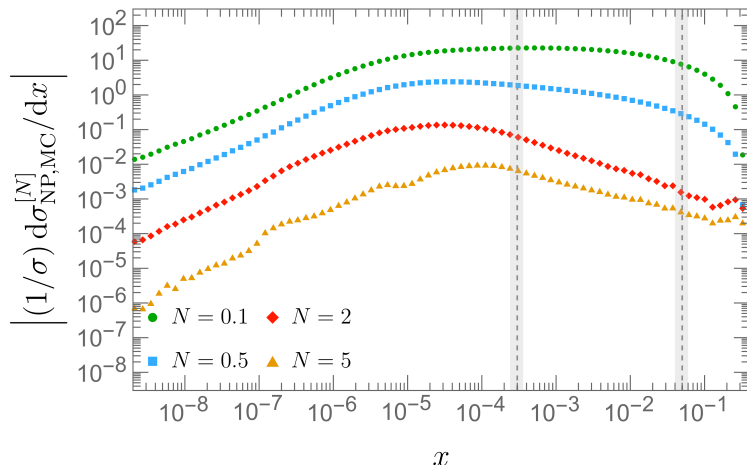


Figure 5: Log-log plot showing the non-perturbative contributions extracted from PYTHIA simulations for $N = 0.1, 0.5, 2$ and 5 . The size of these corrections is significantly larger for $N < 1$ than for $N > 1$ values. Moreover, as can be seen when N approaches 0 , the scaling region does not have a simple power law structure (it's not quite a straight line anymore). The vertical dashed lines represent the perturbative scaling region where leading non-perturbative corrections suffice and can be studied. The light gray band shows the variation of these boundaries by $\pm 20\%$, which will be used in fits.

where the first term on the right is the hadron-level distribution of PENC and the second term is the parton-level distribution obtained by turning off hadronization in PYTHIA.

In fig. 5, we plot the overall size of the non-perturbative contributions obtained from PYTHIA simulations, as defined by eq. (4.9), for $N = 0.1, 0.5, 2$ and 5 . From the figure, we first observe that the overall size of power corrections is larger for smaller values of N , especially when $N < 1$. We show the absolute value for this non-perturbative estimate as for $N < 1$ the difference is negative, consistent with our analytic predictions (see eq. (4.7)). The vertical dashed lines in fig. 5 indicate the fit region used for the estimation of the leading non-perturbative power corrections in our analysis. This region is selected such that the perturbative power law scaling holds in this regime and the non-perturbative corrections can be described sufficiently with the leading contribution. The shaded gray region in the figure shows the variation of this region by $\pm 20\%$.

We start by testing the predicted scaling behavior as function of N for $N > 1$ values. To this end, we take the ratios of non-perturbative corrections extracted from the simulations (see eq. (4.9)) to the corresponding quantity for the two-point energy correlator. From eq. (4.7), the leading non-perturbative power correction then scale as

$$\frac{d\sigma_{\text{NP,MC}}^{[N]}}{d\sigma_{\text{NP,MC}}^{[2]}} \approx \frac{d\sigma_{\text{NP}}^{[N]}}{d\sigma_{\text{NP}}^{[2]}} = \frac{N}{2^{N-1}}. \quad (4.10)$$

The resulting distributions are shown in fig. 6 for $N = 3, 4, 5$, and 10 relative to $N = 2$, plotted as a function of x . The horizontal dashed lines correspond to the leading

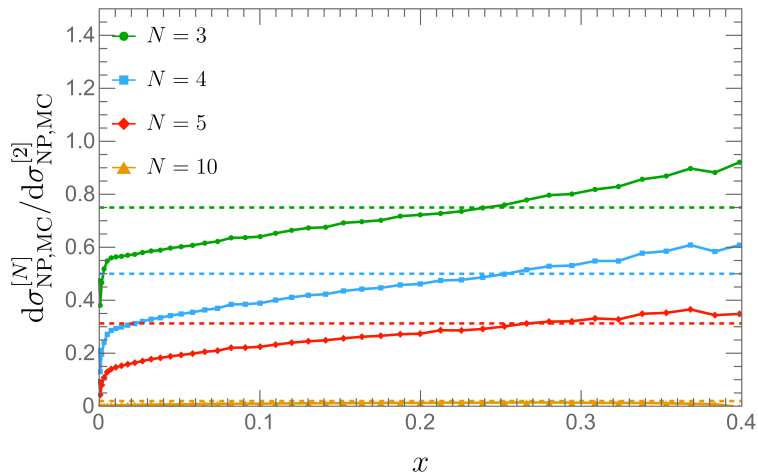


Figure 6: The difference between hadron level and parton level distributions, for $N = 3, 4, 5, 10$, normalized to the same quantity for $N = 2$. The horizontal dashed lines indicate leading order theoretical predictions.

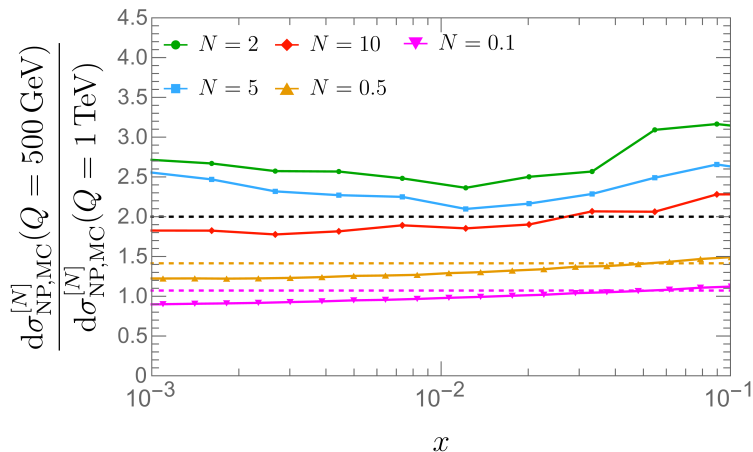


Figure 7: Ratio of the non-perturbative corrections at two different center-of-mass energies, $Q = 500 \text{ GeV}$ and $Q = 1 \text{ TeV}$ for various N -values ($N = 0.1, 0.5, 2, 5, 10$). The dashed lines represent the expected analytic prediction in eqs. (4.11) and (4.12). For $N > 1$, deviations from the classical scaling are clearly visible, while for $N < 1$ the simulated data is well-described by the predicted classical scaling.

order theoretical predictions. From the figure we find that the leading power-corrections are close to the theoretically predicted values, but the simulated results from PYTHIA are not constant but depend on x . This shape of the power corrections emerges from the RGE of the jet function in the collinear region, which induces an anomalous scaling governed by the $N - 1$ collinear partons [37]. We will explore this further in fig. 8.

Next, we test the dependence on center-of-mass energy of these contributions by comparing the ratio of the non-perturbative corrections for a given N at two different values of

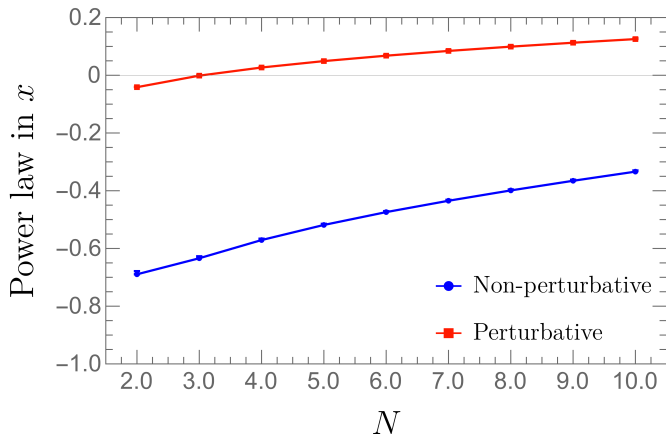


Figure 8: Extracted power law scaling from the log-log plots are shown as a function of N . Both perturbative (red) and non-perturbative (blue) power laws are shown. As N increases, both move upward, reflecting the quantum scaling in N . The fit errors from varying the fit region are found to be tiny for $N > 2$, causing the error bars to be barely visible.

Q , namely $Q = 500$ GeV and $Q = 1$ TeV. The expected scaling in Q for $N > 1$ is simply given as

$$\frac{d\sigma_{\text{NP,MC}}^{[N]}(Q = 500 \text{ GeV})}{d\sigma_{\text{NP,MC}}^{[N]}(Q = 1 \text{ TeV})} \approx \frac{d\sigma_{\text{NP}}^{[N]}(Q = 500 \text{ GeV})}{d\sigma_{\text{NP}}^{[N]}(Q = 1 \text{ TeV})} = 2, \quad (4.11)$$

while for $N < 1$, the leading power corrections exhibit a Q dependence governed by

$$\frac{d\sigma_{\text{NP,MC}}^{[N]}(Q = 500 \text{ GeV})}{d\sigma_{\text{NP,MC}}^{[N]}(Q = 1 \text{ TeV})} \approx \frac{d\sigma_{\text{NP}}^{[N]}(Q = 500 \text{ GeV})}{d\sigma_{\text{NP}}^{[N]}(Q = 1 \text{ TeV})} = 2^N. \quad (4.12)$$

The results are shown in fig. 7 for $N = 0.1, 0.5, 2, 5, 10$. Although the predicted dependence on the center-of-mass energy is well described for $N < 1$, the resulting distributions show clear deviations from the fixed-order (classical scaling) prediction for $N > 1$ values. This could be attributed to the fact that for $N < 1$, the overall size of non-perturbative effects is large and any violation of the classical scaling is a smaller effect than the differences between the classical scaling for different N . Meanwhile for $N > 1$, the classical scaling is identical, so differences between different N would be completely due to quantum corrections.

We will now test the dependence of the power corrections on the angular scale x for $N > 1$ correlators. From our leading order predictions, we expect this to scale as

$$\log_{10} \left(\frac{d\sigma_{\text{NP}}^{[N]}}{d \log_{10} x} \right) = -\frac{1}{2} \log_{10} x + \text{constant} \quad (4.13)$$

independent of N . To test this scaling, we use the region indicated in fig. 5 and fit the resulting distribution with a straight line to obtain the power law of the fitted distribution for different N values. We show the extracted power law for both the parton-level distri-

butions and non-perturbative contributions in fig. 8. The fit errors are obtained by varying the fit region by $\pm 20\%$, they are shown in the figure but found to be small. From this figure, we observe that the extracted slope of the power corrections exhibits a dependence on N , contrary to the fixed-order predictions. Interestingly, we find that the N -dependence of this power law for the non-perturbative contributions has a similar shape as for the perturbative (parton-level) distributions, giving evidence of the modification of the power corrections through anomalous scaling and qualitatively following [37]

$$\gamma_{\text{NP}}^{[N]} = -\frac{1}{2} + \hat{\gamma}^{[N-1]} \quad \text{for } N > 1. \quad (4.14)$$

Here $\gamma_{\text{NP}}^{[N]}$ is the anomalous dimensions for the non-perturbative power corrections and $\hat{\gamma}^{[N-1]}$ is the anomalous scaling for the perturbative component for the $(N-1)$ -point energy correlator. The extra $-1/2$ is the change in classical scaling for the leading non-perturbative corrections, see eq. (4.7).

For $N < 1$, eq. (4.7) dictates that the non-perturbative contributions exhibit a non-trivial N -dependence already at the leading order, given as

$$\log_{10} \left(\frac{d\sigma_{\text{NP}}^{[N]}}{d \log_{10} x} \right) = -\frac{N}{2} \log_{10} x + \text{constant} \quad (4.15)$$

The fitted power law for different $N < 1$ values is obtained by using the form

$$\log_{10} \left(\frac{1}{\sigma} \frac{d\sigma_{\text{fit}}^{[N];\text{NP,MC}}}{d \log_{10} x} \right) = a^{[N]} + b^{[N]} \log_{10} x \quad (4.16)$$

and is shown in fig. 9 along with the distribution itself, zoomed in the fit region. From the figure we see that the fitted lines agree reasonably well in the scaling regime with the non-perturbative effects extracted from PYTHIA simulations. Next, in fig. 10, we compare the extracted power law $b^{[N]}$ from the fit as a function of N with our theoretical prediction and find them to be in good agreement.

Finally, the constant term $a^{[N]}$ in the fit is related to the non-perturbative parameter $\tilde{\Omega}^{[N]}$ by

$$a^{[N]} \sim \log_{10} \left(\frac{\tilde{\Omega}^{[N]}}{2^N Q^N} \right). \quad (4.17)$$

The result as a function of N is shown in fig. 11. While in general $\langle z_{\text{NP}}^N \rangle \neq \langle z_{\text{NP}} \rangle^N$, if these expectation values are dominated by a single non-perturbative gluon, we expect $\tilde{\Omega}^{[N]}$ to equal $(\Omega_1)^N$. Comparing the extracted values from the fit, we find that $\tilde{\Omega}^{[N]}$ in this approximation is related to the Ω_1 parameter as follows

$$\log_{10} \left(\frac{\tilde{\Omega}^{[N]}}{2^N Q^N} \right) \approx N \log_{10} \left(\frac{\Omega_1}{2Q} \right). \quad (4.18)$$

We now use this approximation to fit Ω_1^{PYTHIA} in the range $0.15 \leq N \leq 0.65$ in fig. 11. As shown, the fit performs quite well, and the value of $\Omega_1^{\text{PYTHIA}} = 0.36 \pm 0.06$ GeV is in the

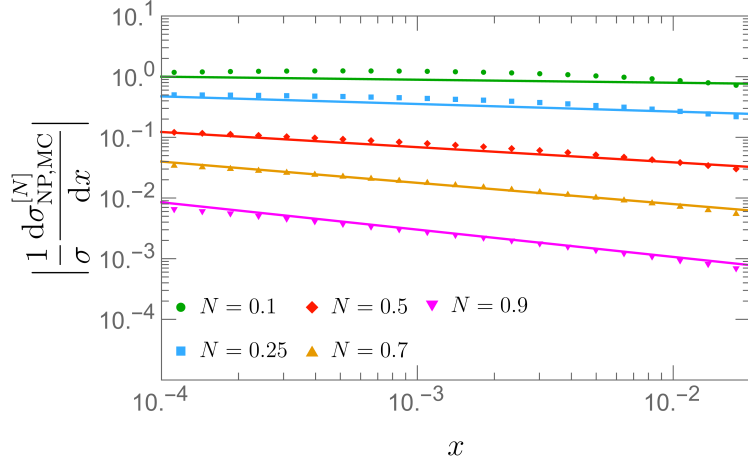


Figure 9: Log-log plot of the non-perturbative distribution, extracted via eq. (4.9), showing the scaling of power corrections with the angular scale x for $N = 0.1, 0.25, 0.5, 0.7$ and 0.9 . The solid straight lines are the fits to a power law in x . The plot is zoomed to the fit region.

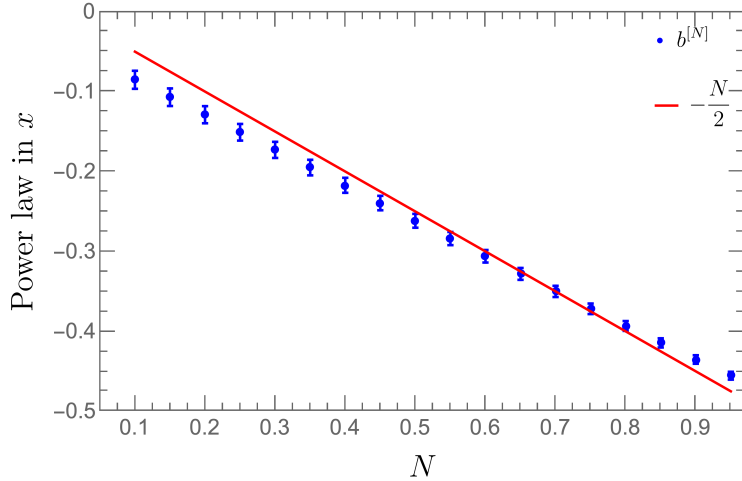


Figure 10: Extracted power law exponent for the dependence on the angular scale x of the power corrections $N < 1$ obtained from the fit in fig. 9. The solid red line shows the theoretical expectation from eq. (4.15).

right ball park. For example, the value $\Omega_1 = 0.305 \pm 0.084$ GeV was obtained from the thrust fit [93], converted to the EEC in ref. [74]. Therefore, we do not find any conclusive evidence that the single non-perturbative gluon approximation is violated for $N < 1$, and thus the leading non-perturbative effect can be described by the same Ω_1 as $N > 1$. As N approaches 1, the first term in eq. (4.7) also contributes and we find that the result deviates from the scaling predicted by considering only the second term, as expected. It is also worth emphasizing that for $N < 1$, these plots suggest that the RGE effects for the non-perturbative power corrections appear to be relatively small.

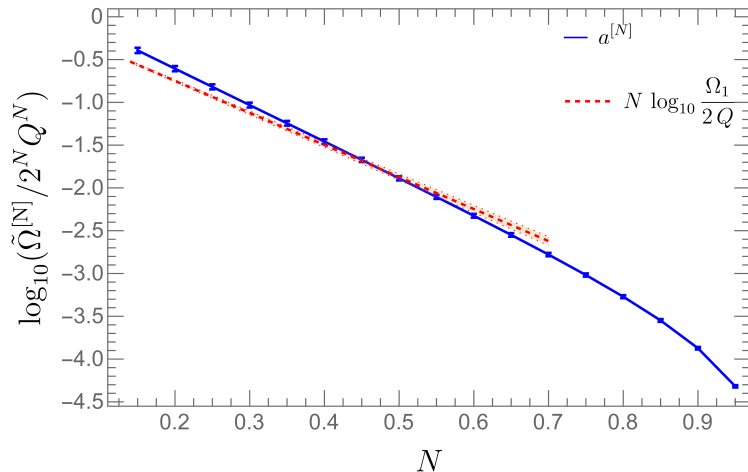


Figure 11: Extracted values of $\tilde{\Omega}^{[N]}$ from the fit compared against the theoretical expectation from a single soft non-perturbative emission.

5 Conclusions

In this work, we study projected N -point energy correlators (PENCs) exploiting the new parametrization introduced by some of us in ref. [52]. Our parametrization organizes the correlator relative to a “special particle” thereby yielding a significantly simpler phase-space that allows computations to be naturally generalized to higher-point correlators in a unified framework. In contrast, for the traditional parametrization each PENC needs to be computed separately as the phase-space becomes increasingly complex for higher values of N . Utilizing this approach, we provide new results in two directions:

First, we derive the factorization formula for general PENC distributions in the back-to-back limit. While the back-to-back limit of the two-point energy correlator has been extensively studied, higher-point correlators have so far not been studied in this regime. This computation is also motivated by experimental considerations as the back-to-back limit provides a complementary phase-space regime with different sources of systematics, that can potentially be used for future determinations of the strong coupling from energy correlators. A key result of our study is the computation of the one-loop jet function for PENCs. Our factorization formula is organized in a way such that the only non-trivial N -dependence resides in one of the jet functions (corresponding to the jet without the special particle in it). We also determine the impact of recoil induced by additional soft radiation that contributes in the back-to-back limit and complicates the determination of which particle is furthest from the special particle. Concretely, we show that the correction to the jet function due to recoil, denoted by ΔJ_{N-1} , is finite and can be computed numerically. Interestingly, we find that in ΔJ_{N-1} the ratio of the coefficient of plus distribution $\Delta \mathcal{F}_{N-1}$ to the constant piece Δj_{N-1} is largely independent of N , though the relative size of the recoil to the no-recoil result *is* N -dependent. Our work provides all the necessary ingredients to carry out the NNLL resummation for higher-point energy correlators.

Second, we study the analytic structure of leading non-perturbative power corrections

to PENC distributions for arbitrary N values, in the collinear limit. For $N > 1$, these power corrections scale linearly in N , consistent with earlier results in the literature [36, 37, 75]. However, we find a new non-perturbative contribution that dominates for $N < 1$ with a different dependence on the angular scale x , a non-trivial dependence on N , and involving a new non-perturbative matrix element $\tilde{\Omega}^{[N]}$. Moreover, we find that the classical scaling is modified to $1/x^{1+N/2}$ for $N < 1$, in contrast to $N > 1$ where classical scaling remains $1/x^{3/2}$ for any N . For $N \rightarrow 0$, this implies that the classical scaling in x of the leading non-perturbative corrections is the same as the (fixed-order) perturbative power law scaling. Using a single soft-gluon approximation, we show that $\tilde{\Omega}^{[N]}$ can be related to the universal non-perturbative parameter Ω_1 that enters in $e^+ e^-$ event shape analyses (including PENCs with $N > 1$). Our analytic predictions are tested against the hadronization model in PYTHIA, finding qualitative agreement everywhere and quantitative agreement in many cases.

The results presented here pave the way for precision analyses with our new parametrization: In the back-to-back limit, the easier phase-space structure directly simplifies the factorization and makes the dependence on N tractable. Non-perturbative corrections in the collinear region are not simplified by our new parametrization, but using our parametrization makes it testable on data, including for non-integer N .

Acknowledgments

We thank Hannah Bossi and Aditya Pathak for helpful discussions, and Johannes Michel and Jesse Thaler for their valuable feedback on the manuscript.

References

- [1] I. Moutl, H. X. Zhu, Energy Correlators: A Journey From Theory to Experiment (6 2025). [arXiv:2506.09119](#).
- [2] P. T. Komiske, I. Moutl, J. Thaler, H. X. Zhu, Analyzing N-Point Energy Correlators inside Jets with CMS Open Data, Phys. Rev. Lett. 130 (5) (2023) 051901. [arXiv:2201.07800](#), [doi:10.1103/PhysRevLett.130.051901](#).
- [3] H. Bossi, et al., Energy Correlators from Partons to Hadrons: Unveiling the Dynamics of the Strong Interactions with Archival ALEPH Data (10 2025). [arXiv:2511.00149](#).
- [4] C. L. Basham, L. S. Brown, S. D. Ellis, S. T. Love, Electron - Positron Annihilation Energy Pattern in Quantum Chromodynamics: Asymptotically Free Perturbation Theory, Phys. Rev. D 17 (1978) 2298. [doi:10.1103/PhysRevD.17.2298](#).
- [5] C. Basham, L. S. Brown, S. D. Ellis, S. T. Love, Energy Correlations in electron - Positron Annihilation: Testing QCD, Phys. Rev. Lett. 41 (1978) 1585. [doi:10.1103/PhysRevLett.41.1585](#).
- [6] C. Basham, L. Brown, S. Ellis, S. Love, Energy Correlations in electron-Positron Annihilation in Quantum Chromodynamics: Asymptotically Free Perturbation Theory, Phys. Rev. D 19 (1979) 2018. [doi:10.1103/PhysRevD.19.2018](#).

- [7] C. L. Basham, L. S. Brown, S. D. Ellis, S. T. Love, Energy Correlations in Perturbative Quantum Chromodynamics: A Conjecture for All Orders, *Phys. Lett. B* 85 (1979) 297–299. [doi:10.1016/0370-2693\(79\)90601-4](https://doi.org/10.1016/0370-2693(79)90601-4).
- [8] D. M. Hofman, J. Maldacena, Conformal collider physics: Energy and charge correlations, *JHEP* 05 (2008) 012. [arXiv:0803.1467](https://arxiv.org/abs/0803.1467), [doi:10.1088/1126-6708/2008/05/012](https://doi.org/10.1088/1126-6708/2008/05/012).
- [9] A. Belitsky, S. Hohenegger, G. Korchemsky, E. Sokatchev, A. Zhiboedov, From correlation functions to event shapes, *Nucl. Phys. B* 884 (2014) 305–343. [arXiv:1309.0769](https://arxiv.org/abs/1309.0769), [doi:10.1016/j.nuclphysb.2014.04.020](https://doi.org/10.1016/j.nuclphysb.2014.04.020).
- [10] J. Henn, E. Sokatchev, K. Yan, A. Zhiboedov, Energy-energy correlation in $N=4$ super Yang-Mills theory at next-to-next-to-leading order, *Phys. Rev. D* 100 (3) (2019) 036010. [arXiv:1903.05314](https://arxiv.org/abs/1903.05314), [doi:10.1103/PhysRevD.100.036010](https://doi.org/10.1103/PhysRevD.100.036010).
- [11] L. J. Dixon, I. Moulton, H. X. Zhu, Collinear limit of the energy-energy correlator, *Phys. Rev. D* 100 (1) (2019) 014009. [arXiv:1905.01310](https://arxiv.org/abs/1905.01310), [doi:10.1103/PhysRevD.100.014009](https://doi.org/10.1103/PhysRevD.100.014009).
- [12] H. Chen, M.-X. Luo, I. Moulton, T.-Z. Yang, X. Zhang, H. X. Zhu, Three point energy correlators in the collinear limit: symmetries, dualities and analytic results, *JHEP* 08 (08) (2020) 028. [arXiv:1912.11050](https://arxiv.org/abs/1912.11050), [doi:10.1007/JHEP08\(2020\)028](https://doi.org/10.1007/JHEP08(2020)028).
- [13] M.-X. Luo, V. Shtabovenko, T.-Z. Yang, H. X. Zhu, Analytic Next-To-Leading Order Calculation of Energy-Energy Correlation in Gluon-Initiated Higgs Decays, *JHEP* 06 (2019) 037. [arXiv:1903.07277](https://arxiv.org/abs/1903.07277), [doi:10.1007/JHEP06\(2019\)037](https://doi.org/10.1007/JHEP06(2019)037).
- [14] H. Chen, I. Moulton, X. Zhang, H. X. Zhu, Rethinking jets with energy correlators: Tracks, resummation, and analytic continuation, *Phys. Rev. D* 102 (5) (2020) 054012. [arXiv:2004.11381](https://arxiv.org/abs/2004.11381), [doi:10.1103/PhysRevD.102.054012](https://doi.org/10.1103/PhysRevD.102.054012).
- [15] H. Chen, I. Moulton, H. X. Zhu, Spinning gluons from the QCD light-ray OPE, *JHEP* 08 (2022) 233. [arXiv:2104.00009](https://arxiv.org/abs/2104.00009), [doi:10.1007/JHEP08\(2022\)233](https://doi.org/10.1007/JHEP08(2022)233).
- [16] H. Bossi, A. Baty, Y. Chen, Y.-C. J. Chen, G.-M. Innocenti, M. Maggi, C. McGinn, Y.-J. Lee, Measurement of the energy-energy correlator in the back-to-back limit using the archived ALEPH $e+e-$ data at 91.2 GeV, *PoS LHCP2024* (2025) 228. [arXiv:2501.01968](https://arxiv.org/abs/2501.01968), [doi:10.22323/1.478.0228](https://doi.org/10.22323/1.478.0228).
- [17] H. Bossi, Y.-C. Chen, Y. Chen, J. Zhang, G. M. Innocenti, A. Badea, A. Baty, M. Maggi, C. McGinn, Y.-J. Lee, Analysis note: measurement of energy-energy correlator in e^+e^- collisions at 91 GeV with archived ALEPH data (5 2025). [arXiv:2505.11828](https://arxiv.org/abs/2505.11828).
- [18] A. Hayrapetyan, et al., Measurement of Energy Correlators inside Jets and Determination of the Strong Coupling $\alpha_S(m_Z)$, *Phys. Rev. Lett.* 133 (7) (2024) 071903. [arXiv:2402.13864](https://arxiv.org/abs/2402.13864), [doi:10.1103/PhysRevLett.133.071903](https://doi.org/10.1103/PhysRevLett.133.071903).
- [19] S. Acharya, et al., Exposing the parton-hadron transition within jets with energy-energy correlators in pp collisions at $\sqrt{s} = 5.02$ TeV (9 2024). [arXiv:2409.12687](https://arxiv.org/abs/2409.12687).
- [20] S. Acharya, et al., Energy-energy correlators in charm-tagged jets in proton-proton collisions at $\sqrt{s} = 13$ TeV (4 2025). [arXiv:2504.03431](https://arxiv.org/abs/2504.03431).
- [21] B. E. Aboona, et al., Measurement of Two-Point Energy Correlators within Jets in $p + p$ Collisions at $\sqrt{s} = 200$ GeV, *Phys. Rev. Lett.* 135 (11) (2025) 111901. [arXiv:2502.15925](https://arxiv.org/abs/2502.15925), [doi:10.1103/wv2t-dkgn](https://doi.org/10.1103/wv2t-dkgn).
- [22] V. Chekhovsky, et al., Observation of nuclear modification of energy-energy correlators

- inside jets in heavy ion collisions, *Phys. Lett. B* 866 (2025) 139556. [arXiv:2503.19993](#), [doi:10.1016/j.physletb.2025.139556](#).
- [23] C. Collaboration, Energy-energy correlators from PbPb and pp collisions at 5.02 TeV, Preprint (2024) CMS-PAS-HIN-23-004.
- [24] Energy-energy correlation in Z boson tagged PbPb and pp collisions at $\sqrt{s_{NN}} = 5.02$ TeV (2025).
- [25] H.-M. Chang, M. Procura, J. Thaler, W. J. Waalewijn, Calculating Track-Based Observables for the LHC, *Phys. Rev. Lett.* 111 (2013) 102002. [arXiv:1303.6637](#), [doi:10.1103/PhysRevLett.111.102002](#).
- [26] H.-M. Chang, M. Procura, J. Thaler, W. J. Waalewijn, Calculating Track Thrust with Track Functions, *Phys. Rev. D* 88 (2013) 034030. [arXiv:1306.6630](#), [doi:10.1103/PhysRevD.88.034030](#).
- [27] Y. Li, I. Moulton, S. S. van Velzen, W. J. Waalewijn, H. X. Zhu, Extending Precision Perturbative QCD with Track Functions, *Phys. Rev. Lett.* 128 (18) (2022) 182001. [arXiv:2108.01674](#), [doi:10.1103/PhysRevLett.128.182001](#).
- [28] M. Jaarsma, Y. Li, I. Moulton, W. J. Waalewijn, H. X. Zhu, Energy correlators on tracks: resummation and non-perturbative effects, *JHEP* 12 (2023) 087. [arXiv:2307.15739](#), [doi:10.1007/JHEP12\(2023\)087](#).
- [29] M. Jaarsma, Y. Li, I. Moulton, W. J. Waalewijn, H. X. Zhu, From DGLAP to Sudakov: Precision Predictions for Energy-Energy Correlators (12 2025). [arXiv:2512.11950](#).
- [30] J. Holguin, I. Moulton, A. Pathak, M. Procura, New paradigm for precision top physics: Weighing the top with energy correlators, *Phys. Rev. D* 107 (11) (2023) 114002. [arXiv:2201.08393](#), [doi:10.1103/PhysRevD.107.114002](#).
- [31] J. Holguin, I. Moulton, A. Pathak, M. Procura, R. Schöfbeck, D. Schwarz, Using the W as a Standard Candle to Reach the Top: Calibrating Energy Correlator Based Top Mass Measurements (11 2023). [arXiv:2311.02157](#).
- [32] J. Holguin, I. Moulton, A. Pathak, M. Procura, R. Schöfbeck, D. Schwarz, Top quark mass extractions from energy correlators: a feasibility study, *JHEP* 04 (2025) 072. [arXiv:2407.12900](#), [doi:10.1007/JHEP04\(2025\)072](#).
- [33] M. Xiao, Y. Ye, X. Zhu, Prospect of measuring the top quark mass through energy correlators, *JHEP* 10 (2024) 088. [arXiv:2405.20001](#), [doi:10.1007/JHEP10\(2024\)088](#).
- [34] J. Holguin, I. Moulton, A. Pathak, M. Procura, S. Sule, High precision heavy-boson-jet substructure with energy correlators (1 2026). [arXiv:2601.20923](#).
- [35] A. Gao, K. Lee, X. Zhang, Precision Jet Substructure of Boosted Boson Decays with Energy Correlators (1 2026). [arXiv:2601.20933](#).
- [36] H. Chen, P. F. Monni, Z. Xu, H. X. Zhu, Scaling Violation in Power Corrections to Energy Correlators from the Light-Ray Operator Product Expansion, *Phys. Rev. Lett.* 133 (23) (2024) 231901. [arXiv:2406.06668](#), [doi:10.1103/PhysRevLett.133.231901](#).
- [37] K. Lee, A. Pathak, I. W. Stewart, Z. Sun, Nonperturbative Effects in Energy Correlators: From Characterizing Confinement Transition to Improving α_s Extraction, *Phys. Rev. Lett.* 133 (23) (2024) 231902. [arXiv:2405.19396](#), [doi:10.1103/PhysRevLett.133.231902](#).

- [38] E. Craft, K. Lee, B. Meçaj, I. Moult, Beautiful and Charming Energy Correlators (10 2022). [arXiv:2210.09311](#).
- [39] J. Barata, J. Brewer, K. Lee, J. M. Silva, Heavy Quark Pair Energy Correlators: From Profiling Partonic Splittings to Probing Heavy-Flavor Fragmentation (8 2025). [arXiv:2508.19404](#).
- [40] C. Andres, F. Dominguez, R. Kunnawalkam Elayavalli, J. Holguin, C. Marquet, I. Moult, Resolving the Scales of the Quark-Gluon Plasma with Energy Correlators, *Phys. Rev. Lett.* 130 (26) (2023) 262301. [arXiv:2209.11236](#), [doi:10.1103/PhysRevLett.130.262301](#).
- [41] Z. Yang, Y. He, I. Moult, X.-N. Wang, Probing the Short-Distance Structure of the Quark-Gluon Plasma with Energy Correlators, *Phys. Rev. Lett.* 132 (1) (2024) 011901. [arXiv:2310.01500](#), [doi:10.1103/PhysRevLett.132.011901](#).
- [42] H. Bossi, A. S. Kudinoor, I. Moult, D. Pablos, A. Rai, K. Rajagopal, Imaging the wakes of jets with energy-energy-energy correlators, *JHEP* 12 (2024) 073. [arXiv:2407.13818](#), [doi:10.1007/JHEP12\(2024\)073](#).
- [43] J. a. Barata, J. G. Milhano, A. V. Sadofyev, Picturing QCD jets in anisotropic matter: from jet shapes to energy energy correlators, *Eur. Phys. J. C* 84 (2) (2024) 174. [arXiv:2308.01294](#), [doi:10.1140/epjc/s10052-024-12514-1](#).
- [44] J. a. Barata, P. Caucal, A. Soto-Ontoso, R. Szafron, Advancing the understanding of energy-energy correlators in heavy-ion collisions, *JHEP* 11 (2024) 060. [arXiv:2312.12527](#), [doi:10.1007/JHEP11\(2024\)060](#).
- [45] C. Andres, F. Dominguez, J. Holguin, C. Marquet, I. Moult, Seeing beauty in the quark-gluon plasma with energy correlators, *Phys. Rev. D* 110 (3) (2024) L031503. [arXiv:2307.15110](#), [doi:10.1103/PhysRevD.110.L031503](#).
- [46] B. Singh, V. Vaidya, Factorization for energy-energy correlator in heavy ion collision, *JHEP* 06 (2025) 071. [arXiv:2408.02753](#), [doi:10.1007/JHEP06\(2025\)071](#).
- [47] B. Singh, Toward factorization of jet observable in dense media: An EFT approach, *Int. J. Mod. Phys. A* 40 (28) (2025) 2530012. [arXiv:2505.18070](#), [doi:10.1142/S0217751X25300121](#).
- [48] A. Budhraja, B. Singh, Exploiting ν -dependence of projected energy correlators in HICs, *Phys. Lett. B* 872 (2026) 140079. [arXiv:2503.20019](#), [doi:10.1016/j.physletb.2025.140079](#).
- [49] J. Barata, I. Moult, A. V. Sadofyev, J. M. Silva, Dissecting Jet Modification in the QGP with Multi-Point Energy Correlators (3 2025). [arXiv:2503.13603](#).
- [50] J. Barata, J. G. Milhano, A. V. Sadofyev, J. M. Silva, Early-Time Dynamics of Heavy-Ion Collisions through Energy Correlators: celestial blocks and the spacetime structure of out-of-equilibrium QCD matter (12 2025). [arXiv:2512.17009](#).
- [51] J. Barata, Z.-B. Kang, X. Mayo López, J. Penttala, Energy-Energy Correlator for Jet Production in pp and pA Collisions, *Phys. Rev. Lett.* 134 (25) (2025) 251903. [arXiv:2411.11782](#), [doi:10.1103/96xh-bd1w](#).
- [52] S. Alipour-fard, A. Budhraja, J. Thaler, W. J. Waalewijn, New Angles on Energy Correlators, *Phys. Rev. Lett.* 134 (23) (2025) 231902. [arXiv:2410.16368](#), [doi:10.1103/l6nj-2gsh](#).

- [53] C. W. Bauer, S. Fleming, D. Pirjol, I. W. Stewart, An Effective field theory for collinear and soft gluons: Heavy to light decays, *Phys. Rev. D* 63 (2001) 114020. [arXiv:hep-ph/0011336](#), [doi:10.1103/PhysRevD.63.114020](#).
- [54] C. W. Bauer, D. Pirjol, I. W. Stewart, Soft collinear factorization in effective field theory, *Phys. Rev. D* 65 (2002) 054022. [arXiv:hep-ph/0109045](#), [doi:10.1103/PhysRevD.65.054022](#).
- [55] C. W. Bauer, I. W. Stewart, Invariant operators in collinear effective theory, *Phys. Lett. B* 516 (2001) 134–142. [arXiv:hep-ph/0107001](#), [doi:10.1016/S0370-2693\(01\)00902-9](#).
- [56] C. W. Bauer, S. Fleming, D. Pirjol, I. Z. Rothstein, I. W. Stewart, Hard scattering factorization from effective field theory, *Phys. Rev. D* 66 (2002) 014017. [arXiv:hep-ph/0202088](#), [doi:10.1103/PhysRevD.66.014017](#).
- [57] C. Duhr, B. Mistlberger, G. Vita, Four-Loop Rapidity Anomalous Dimension and Event Shapes to Fourth Logarithmic Order, *Phys. Rev. Lett.* 129 (16) (2022) 162001. [arXiv:2205.02242](#), [doi:10.1103/PhysRevLett.129.162001](#).
- [58] J. C. Collins, D. E. Soper, Back-To-Back Jets: Fourier Transform from B to K-Transverse, *Nucl. Phys. B* 197 (1982) 446–476. [doi:10.1016/0550-3213\(82\)90453-9](#).
- [59] J. C. Collins, D. E. Soper, G. F. Sterman, Transverse Momentum Distribution in Drell-Yan Pair and W and Z Boson Production, *Nucl. Phys. B* 250 (1985) 199–224. [doi:10.1016/0550-3213\(85\)90479-1](#).
- [60] D. de Florian, M. Grazzini, The Back-to-back region in e^+e^- energy-energy correlation, *Nucl. Phys. B* 704 (2005) 387–403. [arXiv:hep-ph/0407241](#), [doi:10.1016/j.nuclphysb.2004.10.051](#).
- [61] Z. Tulipánt, A. Kardos, G. Somogyi, Energy–energy correlation in electron–positron annihilation at NNLL + NNLO accuracy, *Eur. Phys. J. C* 77 (11) (2017) 749. [arXiv:1708.04093](#), [doi:10.1140/epjc/s10052-017-5320-9](#).
- [62] A. Kardos, G. Somogyi, Z. Trócsányi, Soft-drop event shapes in electron–positron annihilation at next-to-next-to-leading order accuracy, *Phys. Lett. B* 786 (2018) 313–318. [arXiv:1807.11472](#), [doi:10.1016/j.physletb.2018.10.014](#).
- [63] I. Moult, H. X. Zhu, Simplicity from Recoil: The Three-Loop Soft Function and Factorization for the Energy-Energy Correlation, *JHEP* 08 (2018) 160. [arXiv:1801.02627](#), [doi:10.1007/JHEP08\(2018\)160](#).
- [64] M. A. Ebert, B. Mistlberger, G. Vita, The Energy-Energy Correlation in the back-to-back limit at N³LO and N³LL', *JHEP* 08 (2021) 022. [arXiv:2012.07859](#), [doi:10.1007/JHEP08\(2021\)022](#).
- [65] U. G. Aglietti, G. Ferrera, Heavy quark mass effects in the energy–energy correlation in the back-to-back region, *Eur. Phys. J. C* 85 (3) (2025) 272. [arXiv:2412.02629](#), [doi:10.1140/epjc/s10052-025-13954-z](#).
- [66] U. G. Aglietti, G. Ferrera, Energy-energy correlation in the back-to-back region at N³LL+NNLO in QCD, *Phys. Rev. D* 110 (11) (2024) 114004. [arXiv:2403.04077](#), [doi:10.1103/PhysRevD.110.114004](#).
- [67] Z.-B. Kang, J. Penttala, C. Zhang, Determination of the strong coupling constant and the Collins-Soper kernel from the energy-energy correlator in e^+e^- collisions (10 2024). [arXiv:2410.21435](#).

- [68] A. Pathak, *Precision Top Mass Using Energy Correlators*, QCD@LHC, Oct, 2024 (2024).
URL https://indico.cern.ch/event/1360294/contributions/6144507/attachments/2941385/5167878/Aditya_Pathak_QCD@LHC.pdf
- [69] H. Bossi, *Energy correlators as a probe of QCD from simple to complex systems*, Nikhef Theory Seminar, Amsterdam, Netherlands, Nov. 19, 2024 (2024).
URL https://indico.nikhef.nl/event/6063/attachments/10747/16463/HBossi_NikhefSeminar.pdf
- [70] Y. L. Dokshitzer, A. Lucenti, G. Marchesini, G. P. Salam, On the QCD analysis of jet broadening, *JHEP* 01 (1998) 011. [arXiv:hep-ph/9801324](#),
[doi:10.1088/1126-6708/1998/01/011](#).
- [71] T. Becher, G. Bell, M. Neubert, Factorization and Resummation for Jet Broadening, *Phys. Lett. B* 704 (2011) 276–283. [arXiv:1104.4108](#), [doi:10.1016/j.physletb.2011.09.005](#).
- [72] A. Budhraj, A. Jain, M. Procura, One-loop angularity distributions with recoil using Soft-Collinear Effective Theory, *JHEP* 08 (2019) 144. [arXiv:1903.11087](#),
[doi:10.1007/JHEP08\(2019\)144](#).
- [73] L. G. Almeida, S. D. Ellis, C. Lee, G. Sterman, I. Sung, J. R. Walsh, Comparing and counting logs in direct and effective methods of QCD resummation, *JHEP* 04 (2014) 174.
[arXiv:1401.4460](#), [doi:10.1007/JHEP04\(2014\)174](#).
- [74] S. T. Schindler, I. W. Stewart, Z. Sun, Renormalons in the energy-energy correlator, *JHEP* 10 (2023) 187, [Erratum: *JHEP* 10, 175 (2024)]. [arXiv:2305.19311](#),
[doi:10.1007/JHEP10\(2023\)187](#).
- [75] A. Budhraj, H. Chen, W. J. Waalewijn, ν -point energy correlators with FastEEC: Small-x physics from LHC jets, *Phys. Lett. B* 861 (2025) 139239. [arXiv:2409.12235](#),
[doi:10.1016/j.physletb.2024.139239](#).
- [76] Y. L. Dokshitzer, B. R. Webber, Calculation of power corrections to hadronic event shapes, *Phys. Lett. B* 352 (1995) 451–455. [arXiv:hep-ph/9504219](#),
[doi:10.1016/0370-2693\(95\)00548-Y](#).
- [77] Y. L. Dokshitzer, B. R. Webber, Power corrections to event shape distributions, *Phys. Lett. B* 404 (1997) 321–327. [arXiv:hep-ph/9704298](#), [doi:10.1016/S0370-2693\(97\)00573-X](#).
- [78] G. P. Korchemsky, G. F. Sterman, Power corrections to event shapes and factorization, *Nucl. Phys. B* 555 (1999) 335–351. [arXiv:hep-ph/9902341](#),
[doi:10.1016/S0550-3213\(99\)00308-9](#).
- [79] C. Bierlich, et al., A comprehensive guide to the physics and usage of PYTHIA 8.3, *SciPost Phys. Codeb.* 2022 (2022) 8. [arXiv:2203.11601](#), [doi:10.21468/SciPostPhysCodeb.8](#).
- [80] C. W. Bauer, D. Pirjol, I. W. Stewart, Factorization and endpoint singularities in heavy to light decays, *Phys. Rev. D* 67 (2003) 071502. [arXiv:hep-ph/0211069](#),
[doi:10.1103/PhysRevD.67.071502](#).
- [81] A. Budhraj, W. J. Waalewijn, FastEEC: Fast evaluation of N-point energy correlators, *Phys. Lett. B* 861 (2025) 139276. [arXiv:2406.08577](#),
[doi:10.1016/j.physletb.2025.139276](#).
- [82] T. Becher, G. Bell, Analytic Regularization in Soft-Collinear Effective Theory, *Phys. Lett. B* 713 (2012) 41–46. [arXiv:1112.3907](#), [doi:10.1016/j.physletb.2012.05.016](#).
- [83] J. Collins, *Foundations of perturbative QCD*, Vol. 32, Cambridge University Press, 2013.

- [84] X.-d. Ji, J.-p. Ma, F. Yuan, QCD factorization for semi-inclusive deep-inelastic scattering at low transverse momentum, *Phys. Rev. D* 71 (2005) 034005. [arXiv:hep-ph/0404183](#), [doi:10.1103/PhysRevD.71.034005](#).
- [85] J.-y. Chiu, A. Fuhrer, A. H. Hoang, R. Kelley, A. V. Manohar, Soft-Collinear Factorization and Zero-Bin Subtractions, *Phys. Rev. D* 79 (2009) 053007. [arXiv:0901.1332](#), [doi:10.1103/PhysRevD.79.053007](#).
- [86] J.-y. Chiu, A. Jain, D. Neill, I. Z. Rothstein, The Rapidity Renormalization Group, *Phys. Rev. Lett.* 108 (2012) 151601. [arXiv:1104.0881](#), [doi:10.1103/PhysRevLett.108.151601](#).
- [87] Y. Li, D. Neill, H. X. Zhu, An exponential regulator for rapidity divergences, *Nucl. Phys. B* 960 (2020) 115193. [arXiv:1604.00392](#), [doi:10.1016/j.nuclphysb.2020.115193](#).
- [88] A. V. Manohar, Deep inelastic scattering as $x \rightarrow 1$ using soft collinear effective theory, *Phys. Rev. D* 68 (2003) 114019. [arXiv:hep-ph/0309176](#), [doi:10.1103/PhysRevD.68.114019](#).
- [89] C. W. Bauer, C. Lee, A. V. Manohar, M. B. Wise, Enhanced nonperturbative effects in Z decays to hadrons, *Phys. Rev. D* 70 (2004) 034014. [arXiv:hep-ph/0309278](#), [doi:10.1103/PhysRevD.70.034014](#).
- [90] M. G. Echevarria, I. Scimemi, A. Vladimirov, Unpolarized Transverse Momentum Dependent Parton Distribution and Fragmentation Functions at next-to-next-to-leading order, *JHEP* 09 (2016) 004. [arXiv:1604.07869](#), [doi:10.1007/JHEP09\(2016\)004](#).
- [91] M. Ritzmann, W. J. Waalewijn, Fragmentation in Jets at NNLO, *Phys. Rev. D* 90 (5) (2014) 054029. [arXiv:1407.3272](#), [doi:10.1103/PhysRevD.90.054029](#).
- [92] P. Nason, M. H. Seymour, Infrared renormalons and power suppressed effects in e^+e^- jet events, *Nuclear Physics B* 454 (1) (1995) 291–309. [doi:https://doi.org/10.1016/0550-3213\(95\)00461-Z](#).
- [93] R. Abbate, M. Fickinger, A. H. Hoang, V. Mateu, I. W. Stewart, Thrust at $N^3\text{LL}$ with Power Corrections and a Precision Global Fit for $\alpha_s(m_Z)$, *Phys. Rev. D* 83 (2011) 074021. [arXiv:1006.3080](#), [doi:10.1103/PhysRevD.83.074021](#).
- [94] M. Z. Akrawy, et al., A Measurement of energy correlations and a determination of $\alpha_s(M_{Z^0}^2)$ in e^+e^- annihilations at $\sqrt{s} = 91$ GeV, *Phys. Lett. B* 252 (1990) 159–169. [doi:10.1016/0370-2693\(90\)91098-V](#).
- [95] R. D. St. Denis, Measurement of α_s from the structure of particle clusters produced in hadronic Z decays, in: 26th Rencontres de Moriond: High-energy Hadronic Interactions, 1991, pp. 171–177.
- [96] P. D. Acton, et al., A Determination of $\alpha_s(M_{Z^0})$ at LEP using resummed QCD calculations, *Z. Phys. C* 59 (1993) 1–20. [doi:10.1007/BF01555834](#).
- [97] C. Lee, G. F. Sterman, Momentum Flow Correlations from Event Shapes: Factorized Soft Gluons and Soft-Collinear Effective Theory, *Phys. Rev. D* 75 (2007) 014022. [arXiv:hep-ph/0611061](#), [doi:10.1103/PhysRevD.75.014022](#).
- [98] V. Mateu, I. W. Stewart, J. Thaler, Power Corrections to Event Shapes with Mass-Dependent Operators, *Phys. Rev. D* 87 (1) (2013) 014025. [arXiv:1209.3781](#), [doi:10.1103/PhysRevD.87.014025](#).
- [99] I. W. Stewart, F. J. Tackmann, W. J. Waalewijn, Dissecting Soft Radiation with

Factorization, Phys. Rev. Lett. 114 (9) (2015) 092001. [arXiv:1405.6722](#),
[doi:10.1103/PhysRevLett.114.092001](#).

- [100] A. Ferdinand, K. Lee, A. Pathak, Field-theoretic analysis of hadronization using soft drop jet mass, Phys. Rev. D 108 (11) (2023) L111501. [arXiv:2301.03605](#),
[doi:10.1103/PhysRevD.108.L111501](#).
- [101] A. J. Larkoski, J. Thaler, Unsafe but Calculable: Ratios of Angularities in Perturbative QCD, JHEP 09 (2013) 137. [arXiv:1307.1699](#), [doi:10.1007/JHEP09\(2013\)137](#).